Electronic Supplementary Information (ESI†)

Oxo(corrolato)vanadium(IV) Catalyzed Epoxidation: An Oxo(peroxo)(corrolato)vanadium(V) is the True Catalytic Species

Panisha Nayak, Manisha Nayak, Kiran Meena and Sanjib Kar*

School of Chemical Sciences, National Institute of Science Education and Research (NISER), Bhubaneswar, Khordha,752050, India and Homi Bhabha National Institute, Training School Complex, Anushakti Nagar, Mumbai, 400 094, India

E-mail: sanjib@niser.ac.in

Table S1. UV–Vis. and electrochemical data for **1** and **2**.

Table S2. EPR data for **1** and **2**.

Table S3. Optimization of styrene epoxidation[a] under variable reaction conditions using oxo(corrolato)vanadium(IV) complex, **2** as the catalyst.

Fig. S1 ESI-MS spectrum of oxo[5,10,15- tris(4-cyanophenyl)corrolato] vanadium(IV), **1** in CH_3CN shows the (a) measured spectrum with isotopic distribution pattern (experimental) and (b) isotopic distribution pattern (simulated).

Fig. S2 ESI-MS spectrum of oxo[5,15-bis(4-cyanophenyl)-10-(4-bromophenyl)-corrolato] vanadium(IV), **2** in CH_3CN shows the (a) measured spectrum with isotopic distribution pattern (experimental) and (b) isotopic distribution pattern (simulated).

Fig. S3 Electronic absorption spectrum of **1** in acetonitrile at 298K.

Fig. S4 Electronic absorption spectrum of **2** in acetonitrile at 298K.

Fig. S5 Evolution of the electronic absorption spectra of **1** in the presence of excess triethylamine in CH_3CN.

Fig. S6 FT-IR spectrum of **1** as a KBr pellet.

Fig. S7 FT-IR spectrum of **2** as a KBr pellet.

Fig. S8 Cyclic voltammogram (black solid line) **1** (10^{-3} M) in CH_3CN containing 0.1 M tetrabutylammonium perchlorate (TBAP) at 298 K. The scan rate used was 100 mV s^{-1}. The potentials are *versus* Ag/AgCl.

Fig. S9 Cyclic voltammogram (black solid line) **2** (10^{-3} M) in CH_3CN containing 0.1 M tetrabutylammonium perchlorate (TBAP) at 298 K. The scan rate used was 100 mV s^{-1}. The potentials are *versus* Ag/AgCl.

Fig. S10 X-band EPR spectrum of **2** was recorded in acetonitrile at 298 K. EPR parameters: microwave frequency, 9.438 GHz; incident microwave power, 0.720 mW; modulation frequency, 100.0 kHz; modulation amplitude, 5.0 G; receiver gain, 2×10^2.

Fig. S11 The ^{1}H-NMR spectrum of conversion of styrene to styrene oxide in $CDCl_3$ solution. The reaction was performed in the air.

Fig. S12 The ^{1}H-NMR spectrum of conversion of 4-methylstyrene to 4-methylstyrene oxide in $CDCl_3$ solution. The reaction was performed in the air.

Fig. S13 ^{1}H-NMR spectrum of conversion of 4-chlorostyrene to 4-chlorostyrene oxide in $CDCl_3$ solution. The reaction was performed in the air.

Fig. S14 ^{1}H-NMR spectrum of conversion of cyclohexene to cyclohexene oxide in $CDCl_3$ solution. The reaction was performed in the air.

Fig. S15 ^{1}H-NMR spectrum of conversion of 1-octene to 1,2-epoxyoctane in $CDCl_3$ solution. The reaction was performed in the air.

Fig. S16 ^{1}H-NMR spectrum of conversion of norbornene to norbornene epoxide in $CDCl_3$ solution. The reaction was performed in the air.

Fig. S17 ^{1}H-NMR spectrum of conversion of cyclooctene to cyclooctene oxide in $CDCl_3$ solution. The reaction was performed in air.

Fig. S18 ^{1}H-NMR spectrum of conversion of cyclohexenone to 1,2-epoxycyclohexenone in $CDCl_3$ solution. The reaction was performed in air.

Fig. S19 ^{1}H-NMR spectrum of conversion of 4-bromostyrene to 4-bromostyrene oxide in $CDCl_3$ solution. The reaction was performed in the air.

Fig. S20 ^{1}H-NMR spectrum of conversion of 4-methyl-3-penten-2-one to 4-methyl-3-penten-2-one oxide in $CDCl_3$ solution. The reaction was performed in air.

Fig. S21 ^{1}H-NMR spectrum of conversion of 2-Cyclopenten-1-one to 2-Cyclopenten-1-one oxide in $CDCl_3$ solution. The reaction was performed in air.

Fig. S22 ^{1}H-NMR spectrum of conversion of *trans*-stilbene to *trans*-stilbene oxide in $CDCl_3$ solution. The reaction was performed in the air.

Fig. S23 ^{1}H-NMR spectrum of conversion of 6-bromo-1-hexene to 6-bromo-1-hexene oxide in $CDCl_3$ solution. The reaction was performed in air.

Fig. S24 ^{1}H-NMR spectrum of conversion of 1-hexene to 1-hexene oxide in $CDCl_3$ solution. The reaction was performed in air.

Fig. S25 ^{1}H-NMR spectrum of conversion of 3-bromopropene to 3-bromopropene oxide in $CDCl_3$ solution. The reaction was performed in air.

Fig. S26 ^{1}H-NMR spectrum of conversion of 4-*tert*-butoxystyrene to 4-*tert*-butoxystyrene oxide in $CDCl_3$ solution. The reaction was performed in air.

Fig. S27 ^{1}H-NMR spectrum of conversion of 4-vinylaniline to 4-vinylaniline oxide in $CDCl_3$ solution. The reaction was performed in air.

Fig. S28 ^{1}H-NMR spectrum of conversion of 4-vinylnapthalene to 4-vinylnapthalene oxide in $CDCl_3$ solution. The reaction was performed in air.

Fig. S29 ^{1}H-NMR spectrum of conversion of 4-nitrostyrene to 4-nitrostyrene oxide in $CDCl_3$ solution. The reaction was performed in air.

Fig. S30 Time evolution UV−vis spectra of the epoxide formation reaction performed at 50°C under air using complex **1** as catalyst.

Fig. S31 Electronic absorption spectrum of **1** (red line) and the green intermediate (green line) in acetonitrile. After performing the reaction at 50°C, the pure green intermediate was purified by column chromatography.

Fig. S32 Time evolution ^{1}H-NMR spectra in CD_3CN of the epoxide formation reaction performed at 50°C under air using complex **1** as catalyst.

Fig. S33 FT-IR spectrum of **1** (red line) and the green intermediate (green line) as KBr pellet. After performing the reaction at 50°C, the pure green intermediate was purified by column chromatography.

Fig. S34 ESI-MS spectrum of green intermediate, oxo(peroxo)(corrolato)vanadium(V) in CH_3CN shows the (a) isotopic distribution pattern (simulated) and (b) measured spectrum with isotopic distribution pattern (experimental).

Fig. S35 ^{1}H-NMR spectrum of styrene oxide in $CDCl_3$ solution.

Fig. S36 ^{13}C {^{1}H}-NMR spectrum of styrene oxide in $CDCl_3$ solution.

Fig. S37 ^{1}H-NMR spectrum of cyclohexene oxide in $CDCl_3$ solution.

Fig. S38 ^{13}C {^{1}H}-NMR spectrum of cyclohexene oxide in $CDCl_3$ solution.

Fig. S39 ^{1}H-NMR spectrum of cyclooctene oxide in $CDCl_3$ solution.

Fig. S40 ^{13}C {^{1}H}-NMR spectrum of cyclooctene oxide in $CDCl_3$ solution.

Table S1. UV-Vis. and electrochemical data for **1** and **2**.

Compound	UV−vis. Data [a] λ_{max} / nm (ε / $M^{-1}cm^{-1}$)	Electrochemical data[a,b]	
		Oxidation E^0, V (ΔE_p, mV)	Reduction E^0, V (ΔE_p, mV)
1	437 (128500), 541 (9200), 606 (29700).	+ 0.36, + 0.52	-0.72
2	433 (120800), 546 (15400), 610 (39900).	+ 0.38, + 0.54	-0.71

[a] In acetonitrile.

[b] The potentials are *versus* Ag/AgCl.

Table S2. EPR data for **1** and **2**.

Compound	g_{iso}	A_{iso}(G)	**ΔH (G)**
1	2.01509	88	20
2	1.97462	86	24

Table S3. Optimization of styrene epoxidation[a] under variable reaction conditions using oxo(corrolato)vanadium(IV) complex, **2** as the catalyst.

Entry	Catalyst (µmol)	Styrene (mmol)	Oxidant (mmol)	Solvent (mL /ratio)	Time (h)	Temp. (˚C)	% Conv.[c]
1	-	5	H_2O_2, 15	MeCN, 5	6	50	12
2	1	5	H_2O_2, 15	MeCN, 5	5	RT	0
3	1	5	H_2O_2, 15	MeCN, 5	5	60	71
4	1	5	H_2O_2, 15	MeCN, 5	5	40	66
5	1	5	TBHP, 15	MeCN:H_2O, 3:2	1	50	45
6	1	5	H_2O_2, 15	MeCN:H_2O, 3:2	0.5	50	24
7	**1**	**5**	**H_2O_2, 15**	**MeCN:H_2O, 3:2**	**1**	**50**	**82**
8	1	5	H_2O_2, 10	MeCN:H_2O, 3:2	1	50	79
9	1	5	H_2O_2, 5	MeCN:H_2O, 3:2	1	50	54
10	1	10	H_2O_2, 15	MeCN:H_2O, 3:2	1	50	41
11	1	15	H_2O_2, 15	MeCN:H_2O, 3:2	1	50	33
[b]**12**	1	5	H_2O_2, 15	MeCN:H_2O, 3:2	1	50	75

[a] Under air, Amount of $KHCO_3$ used = 150 mg (1.5 mmol). [b] under nitrogen atmosphere. [c] % of conversion was established by ^{1}H NMR.

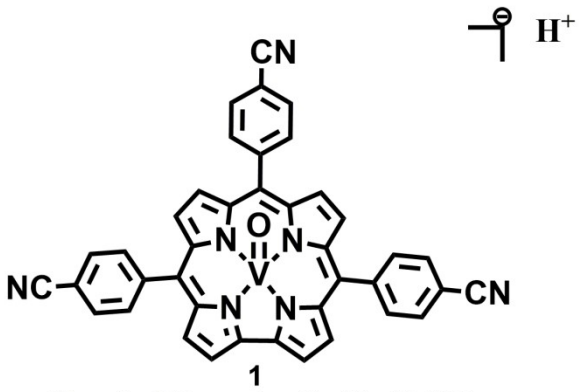

1

Chemical Formula: $C_{40}H_{21}N_7OV$

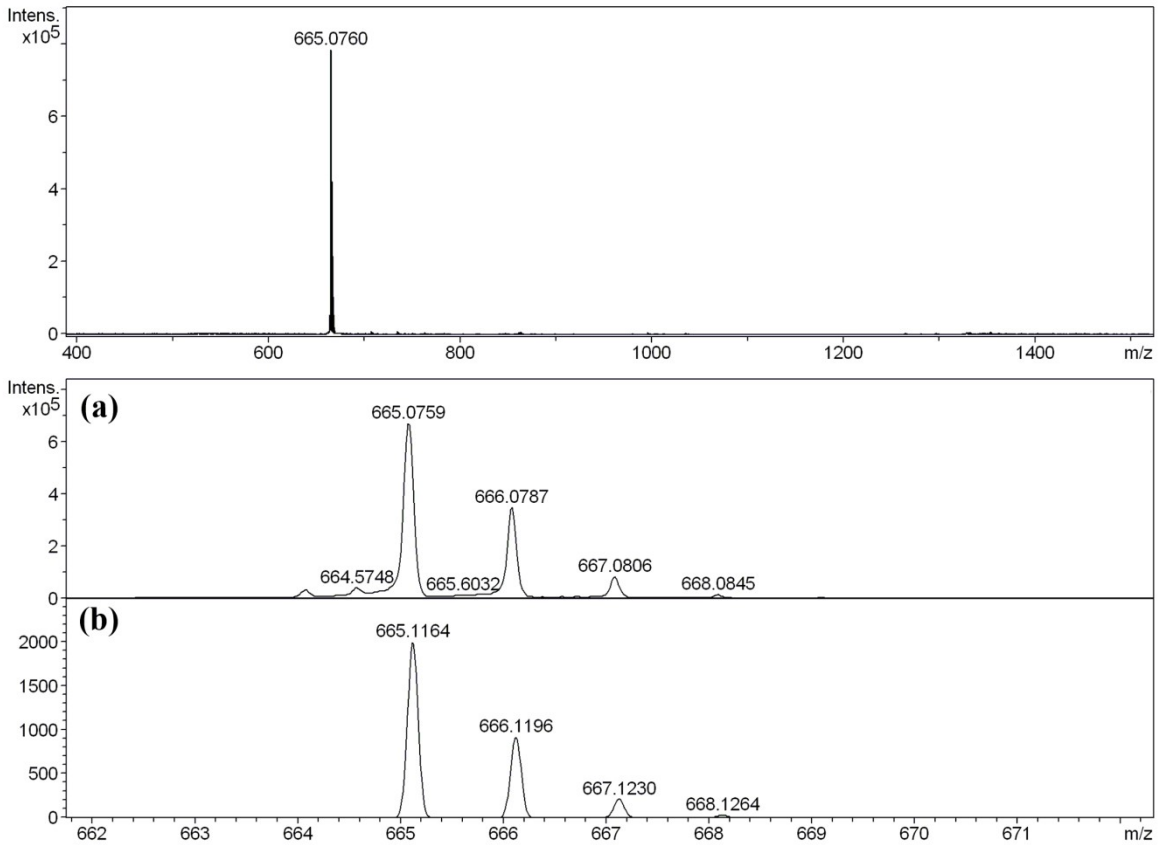

Fig. S1 ESI-MS spectrum of oxo[5,10,15- tris(4-cyanophenyl)corrolato] vanadium (IV), **1** in CH_3CN shows the (a) measured spectrum with isotopic distribution pattern (experimental) and (b) isotopic distribution pattern (simulated).

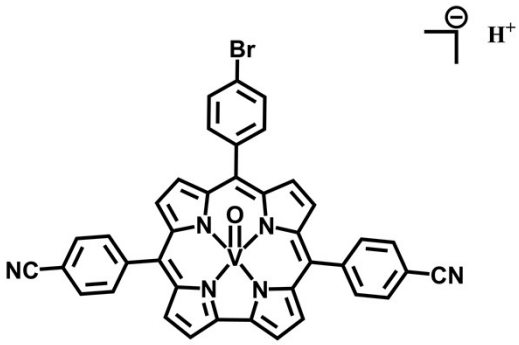

Chemical Formula: $C_{39}H_{20}BrN_6OV$

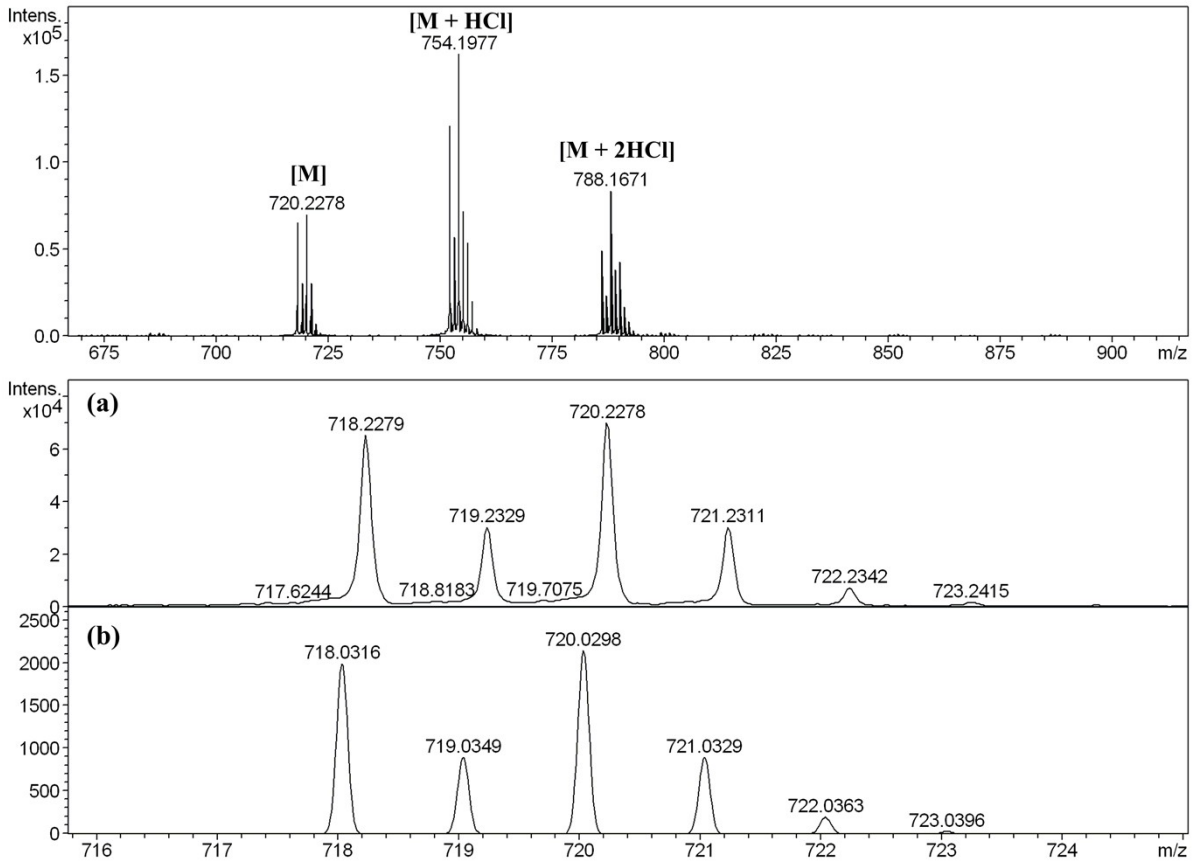

Fig. S2 ESI-MS spectrum of oxo[5,15-bis(4-cyanophenyl)-10-(4-bromophenyl)-corrolato] vanadium (IV), **2** in CH_3CN shows the (a) measured spectrum with isotopic distribution pattern (experimental) and (b) isotopic distribution pattern (simulated).

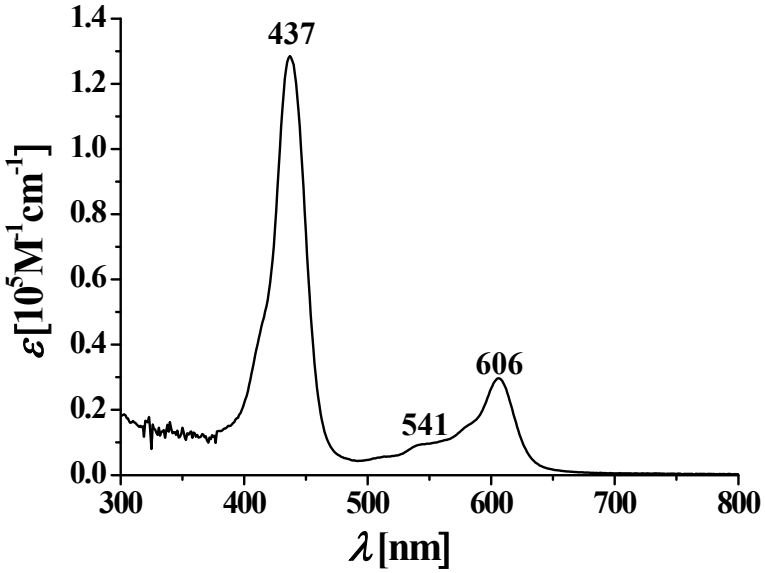

Fig. S3 Electronic absorption spectrum of **1** in acetonitrile at 298K.

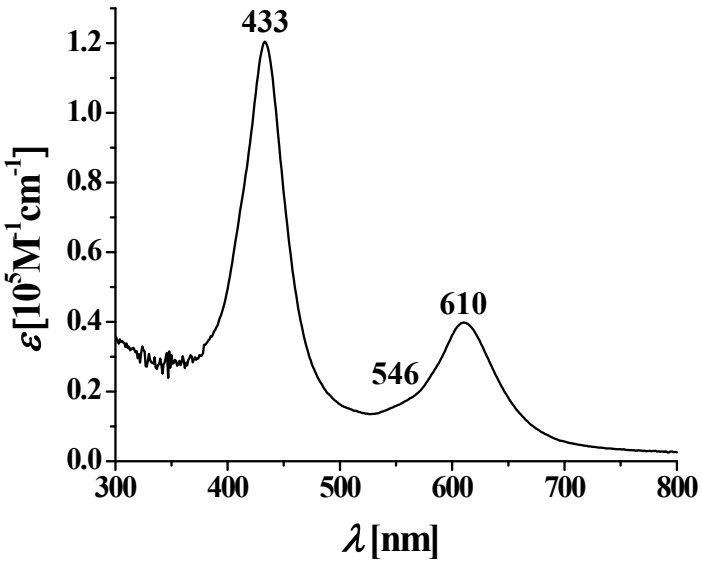

Fig. S4 Electronic absorption spectrum of **2** in acetonitrile at 298K.

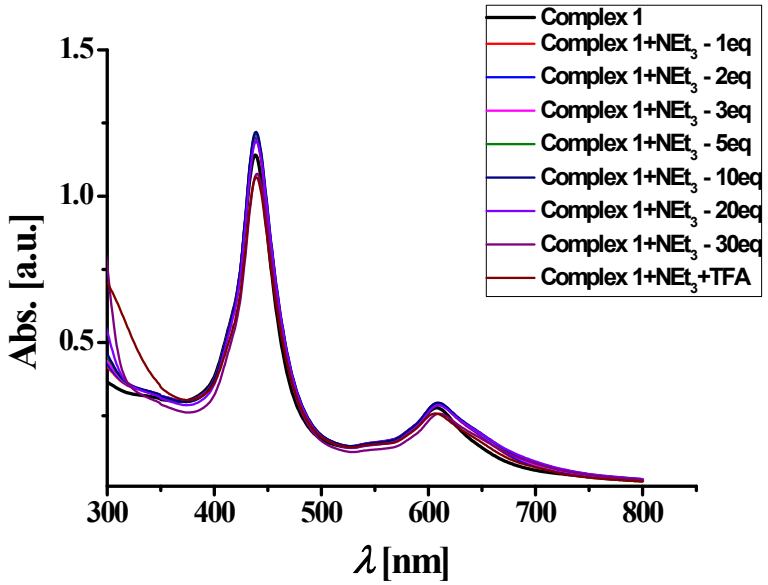

Fig. S5 Evolution of the electronic absorption spectra of **1** in the presence of excess triethylamine in CH_3CN.

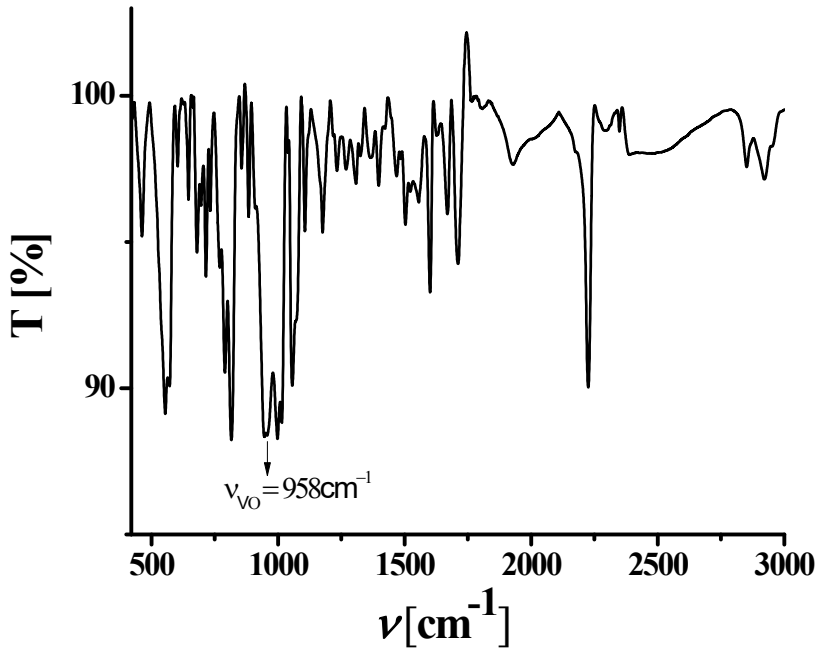

Fig. S6 FT-IR spectrum of **1** as a KBr pellet.

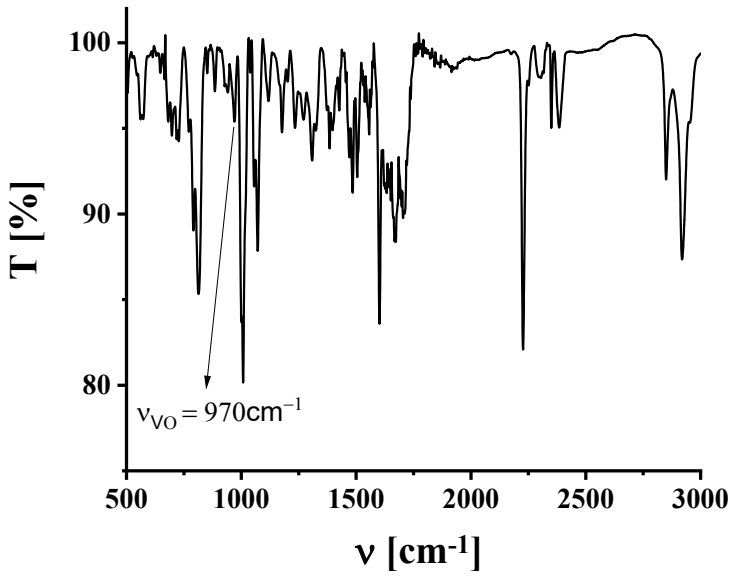

Fig. S7 FT-IR spectrum of **2** as a KBr pellet.

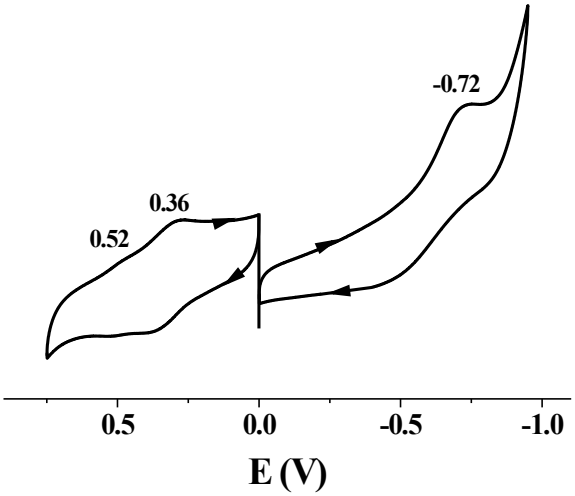

Fig. S8 Cyclic voltammogram (black solid line) **1** (10^{-3} M) in CH_3CN containing 0.1 M tetrabutylammonium perchlorate (TBAP) at 298 K. The scan rate used was 100 mV s^{-1}. The potentials are *versus* Ag/AgCl.

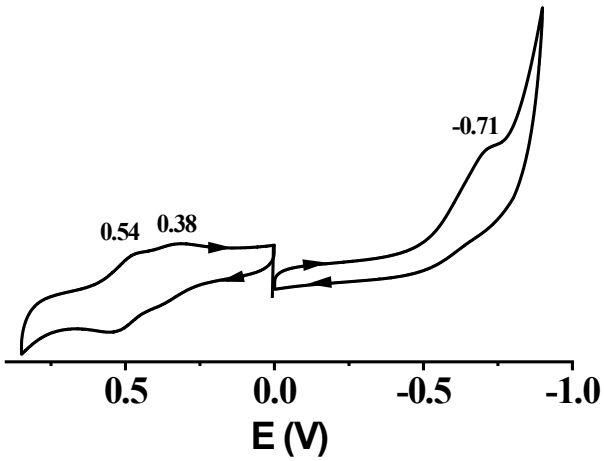

Fig. S9 Cyclic voltammogram (black solid line) **2** (10^{-3} M) in CH_3CN containing 0.1 M tetrabutylammonium perchlorate (TBAP) at 298 K. The scan rate used was 100 mV s^{-1}. The potentials are *versus* Ag/AgCl.

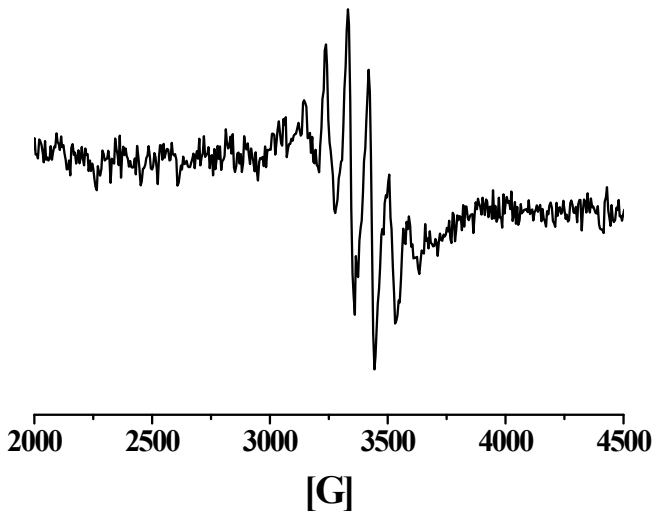

Fig. S10 X-band EPR spectrum of **2** was recorded in acetonitrile at 298 K. EPR parameters: microwave frequency, 9.438 GHz; incident microwave power, 0.720 mW; modulation frequency, 100.0 kHz; modulation amplitude, 5.0 G; receiver gain, 2×10^2.

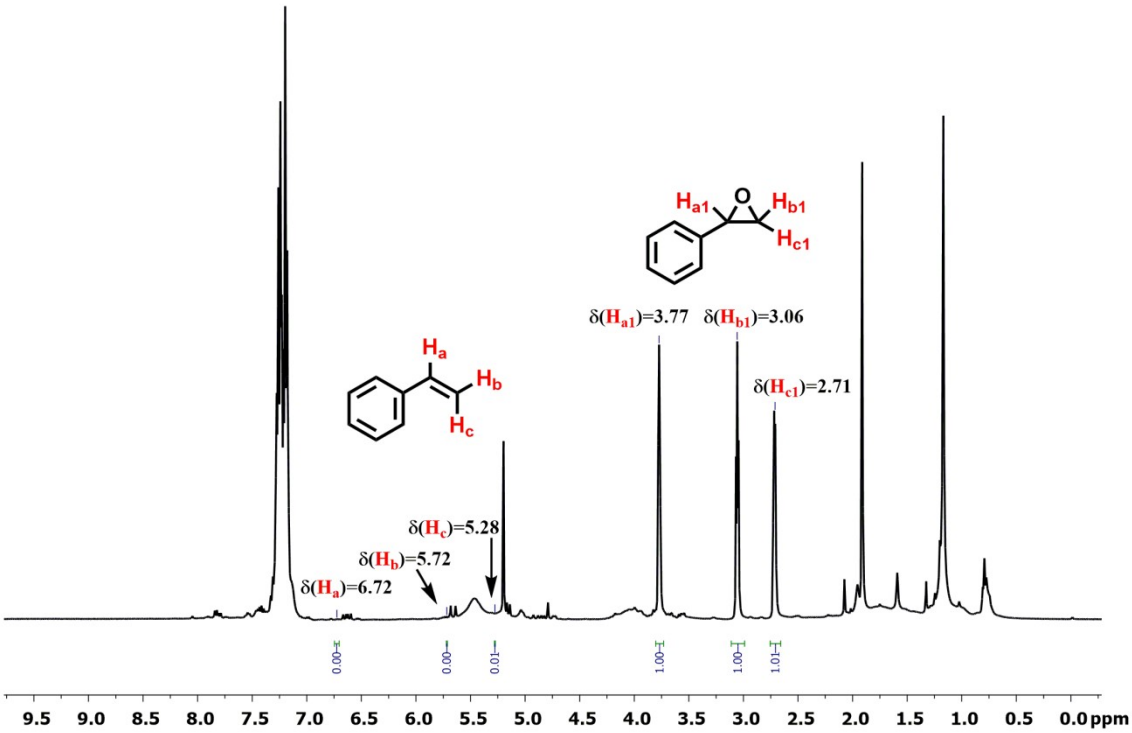

Fig. S11 ^{1}H-NMR spectrum of conversion of styrene to styrene oxide in $CDCl_3$ solution. The reaction was performed in the air.

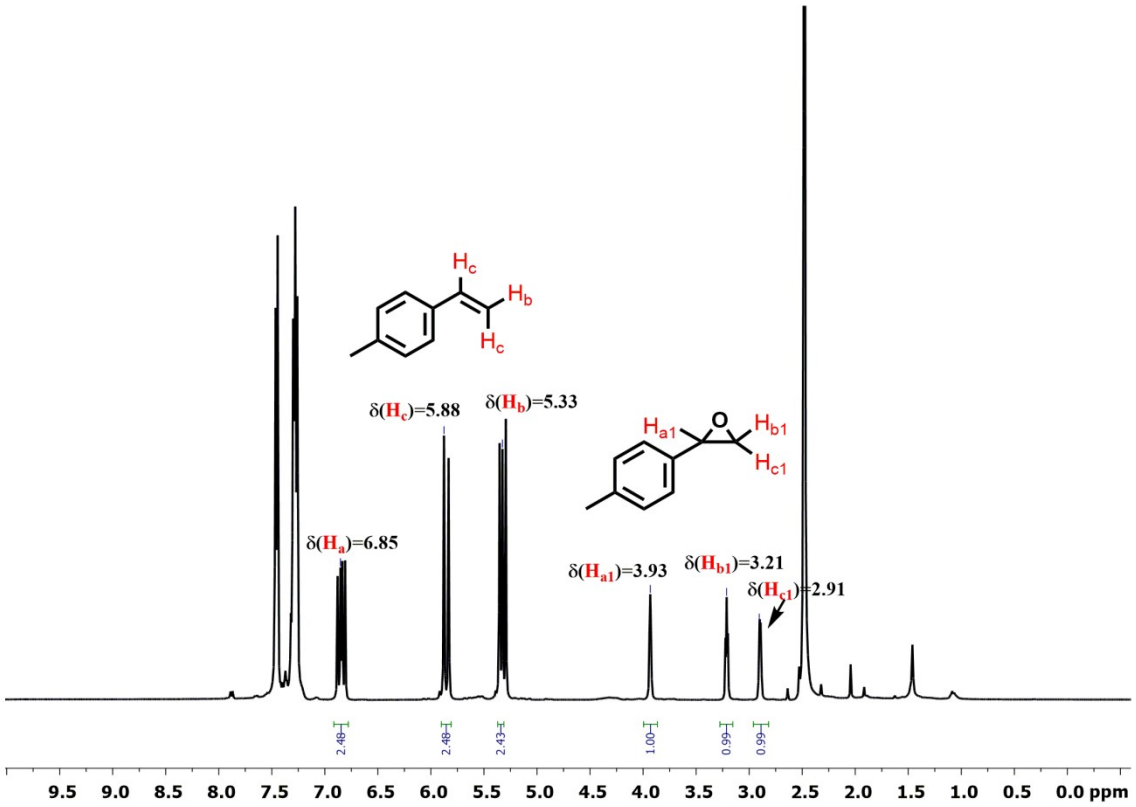

Fig. S12 ^{1}H-NMR spectrum of conversion of 4-methylstyrene to 4-methylstyrene oxide in $CDCl_3$ solution. The reaction was performed in air.

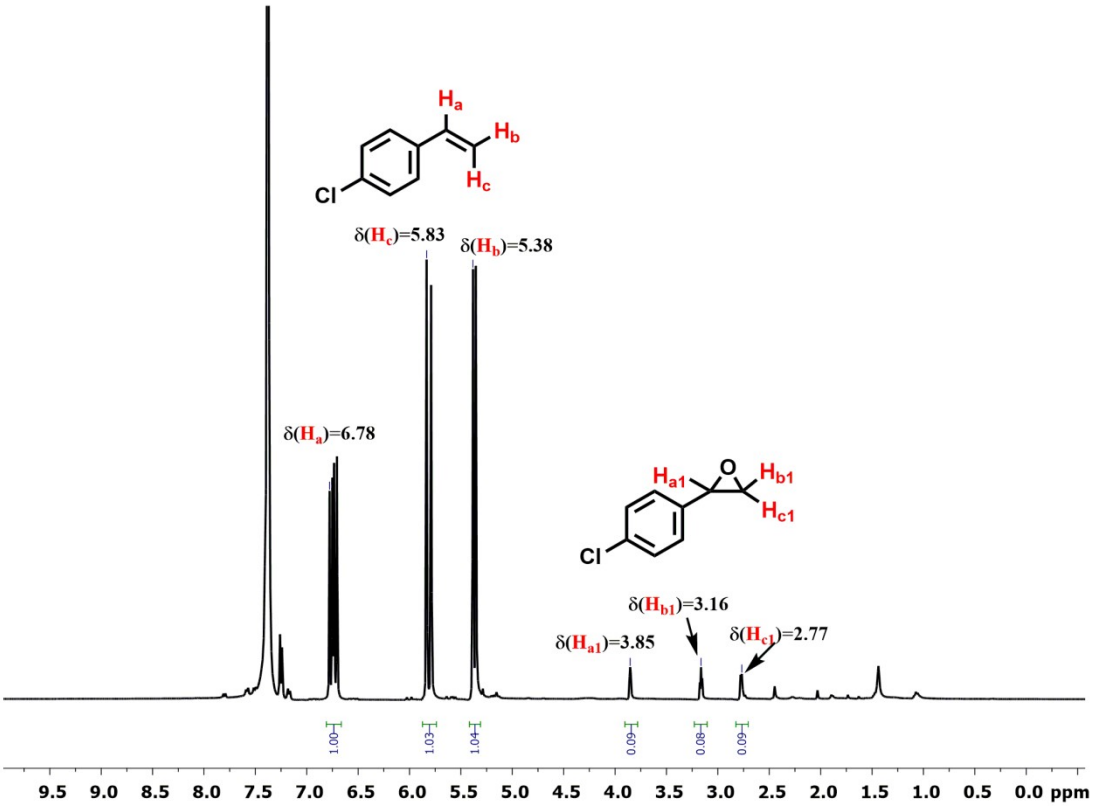

Fig. S13 ^{1}H-NMR spectrum of conversion of 4-chlorostyrene to 4-chlorostyrene oxide in $CDCl_3$ solution. The reaction was performed in air.

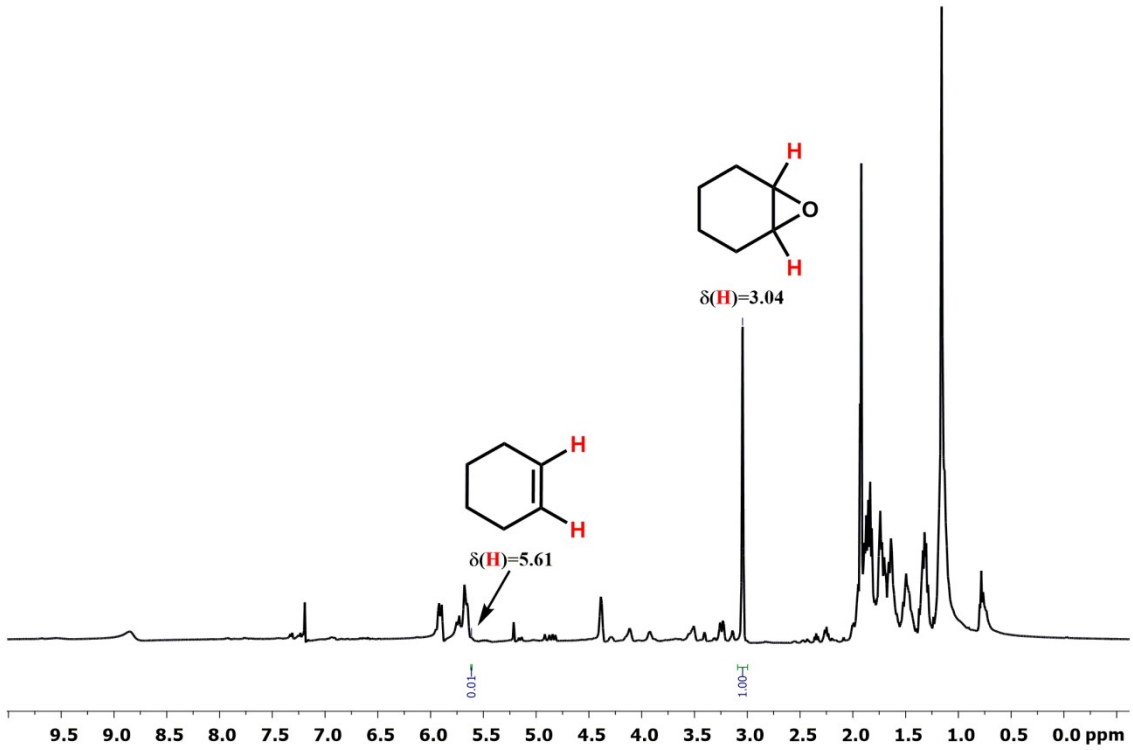

Fig. S14 ^{1}H-NMR spectrum of conversion of cyclohexene to cyclohexene oxide in $CDCl_3$ solution. The reaction was performed in air.

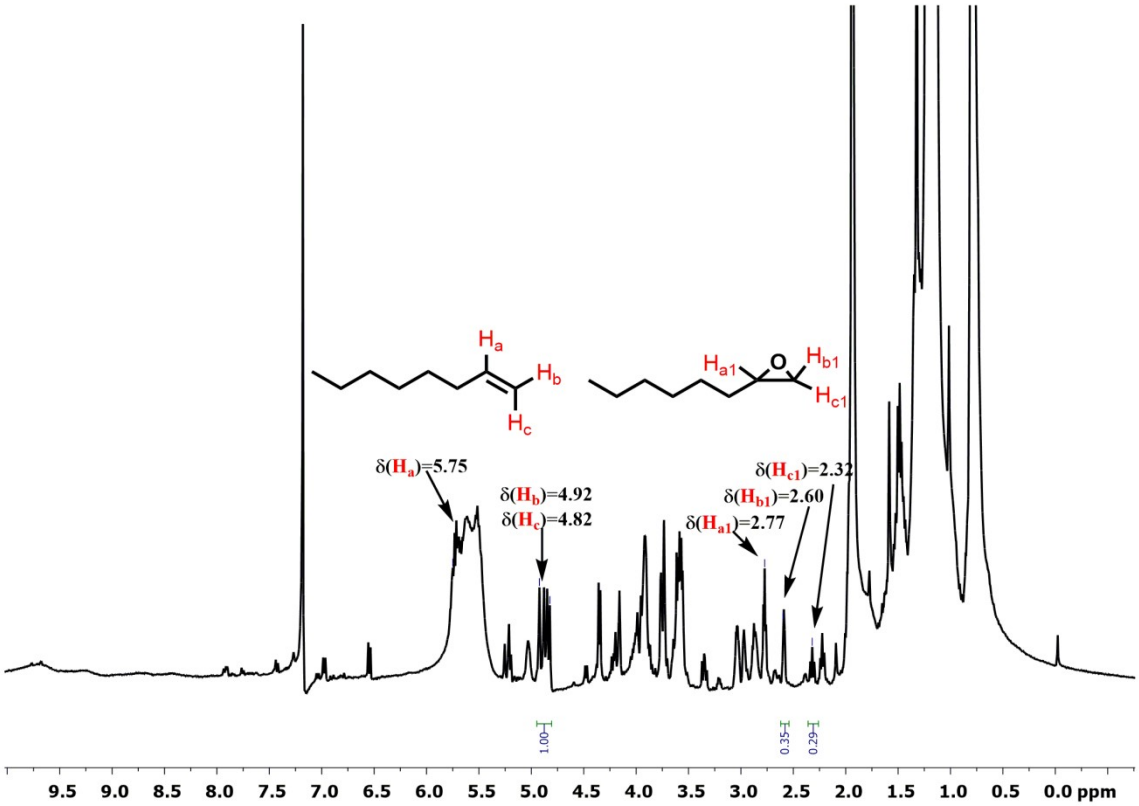

Fig. S15 ^{1}H-NMR spectrum of conversion of 1-octene to 1,2-epoxyoctane in $CDCl_3$ solution. The reaction was performed in air.

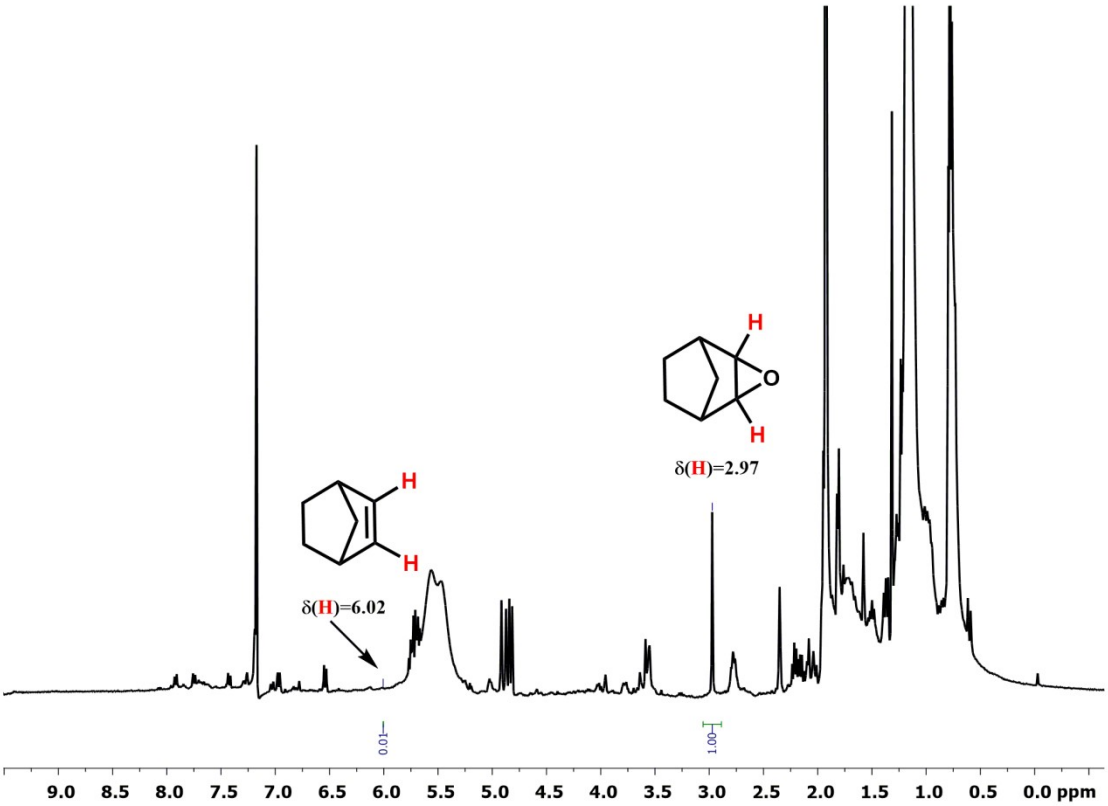

Fig. S16 ^{1}H-NMR spectrum of conversion of norbornene to norbornene epoxide in $CDCl_3$ solution. The reaction was performed in air.

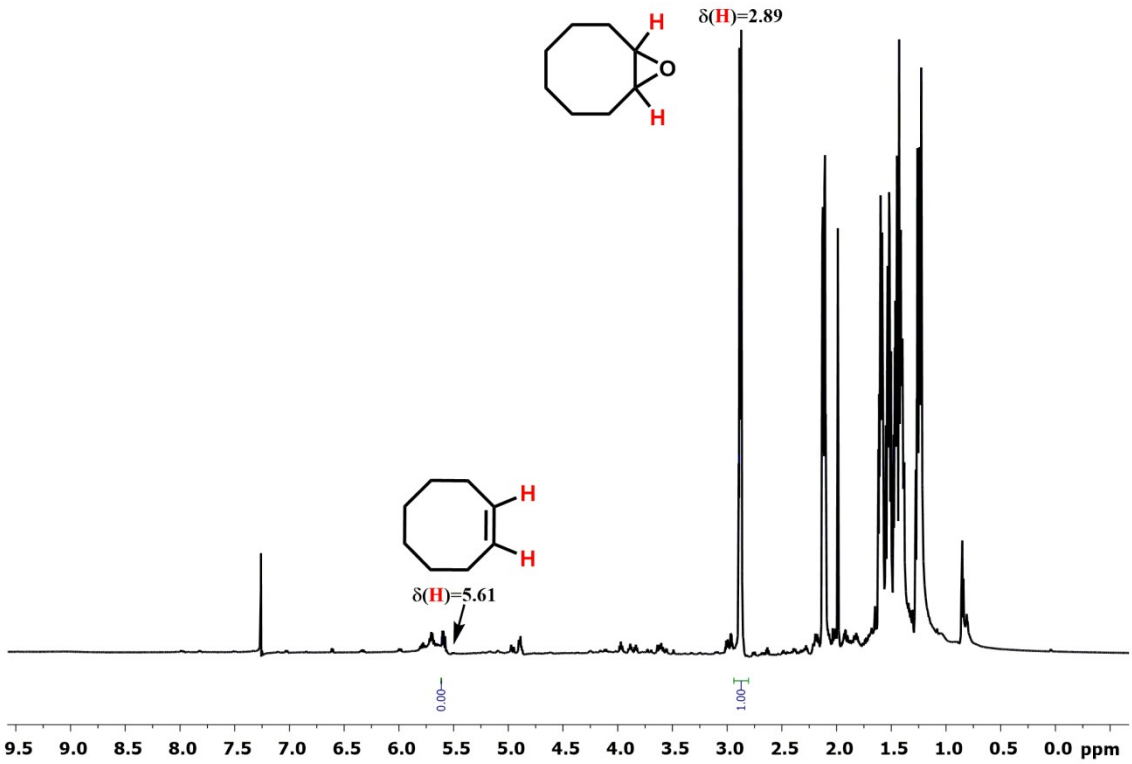

Fig. S17 ^{1}H-NMR spectrum of conversion of cyclooctene to cyclooctene oxide in $CDCl_3$ solution. The reaction was performed in air.

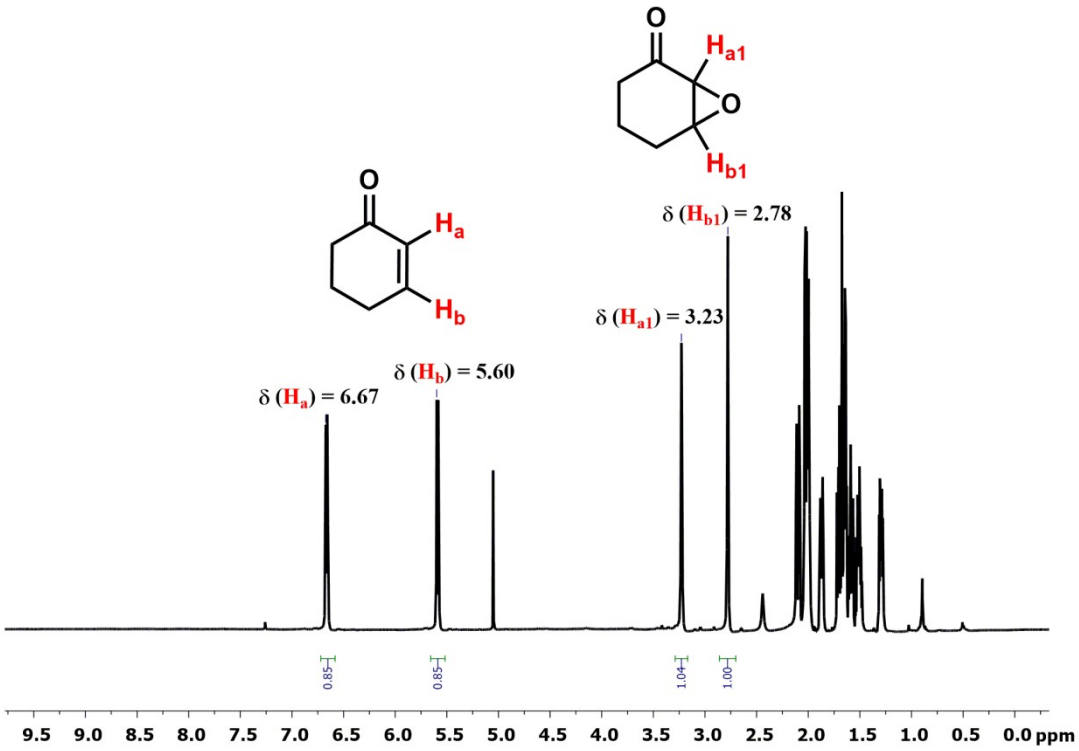

Fig. S18 ^{1}H-NMR spectrum of conversion of cyclohexenone to 1,2-epoxycyclohexenone in $CDCl_3$ solution. The reaction was performed in air.

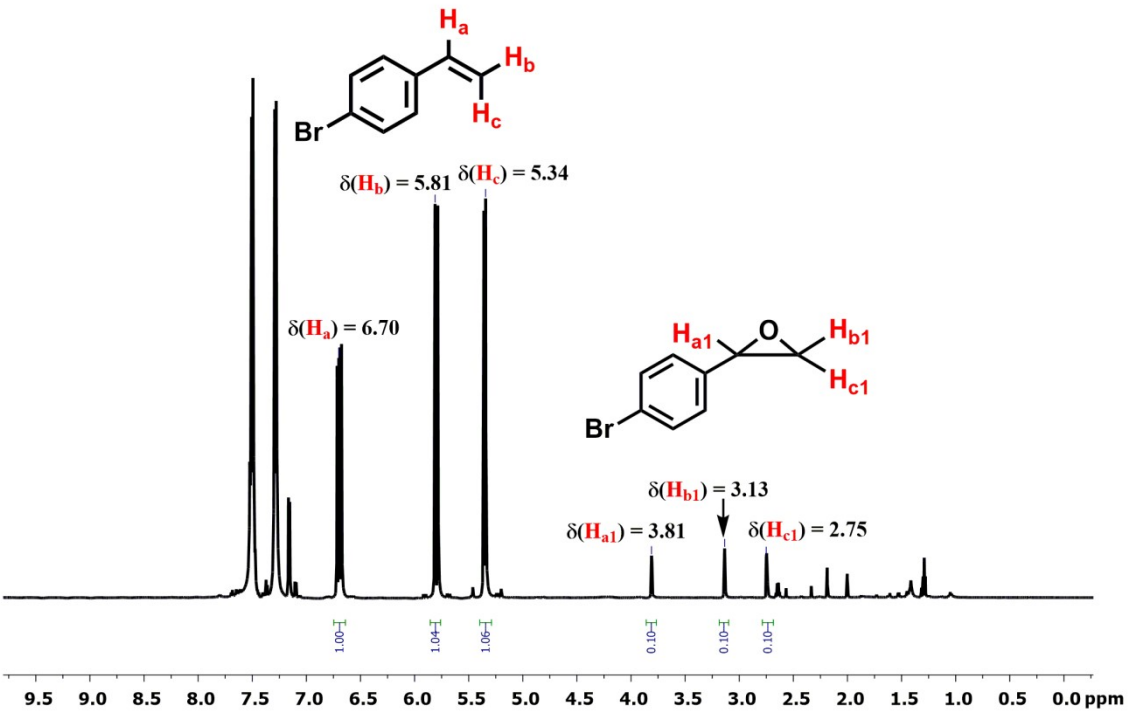

Fig. S19 ^{1}H-NMR spectrum of conversion of 4-bromostyrene to 4-bromostyrene oxide in $CDCl_3$ solution. The reaction was performed in air.

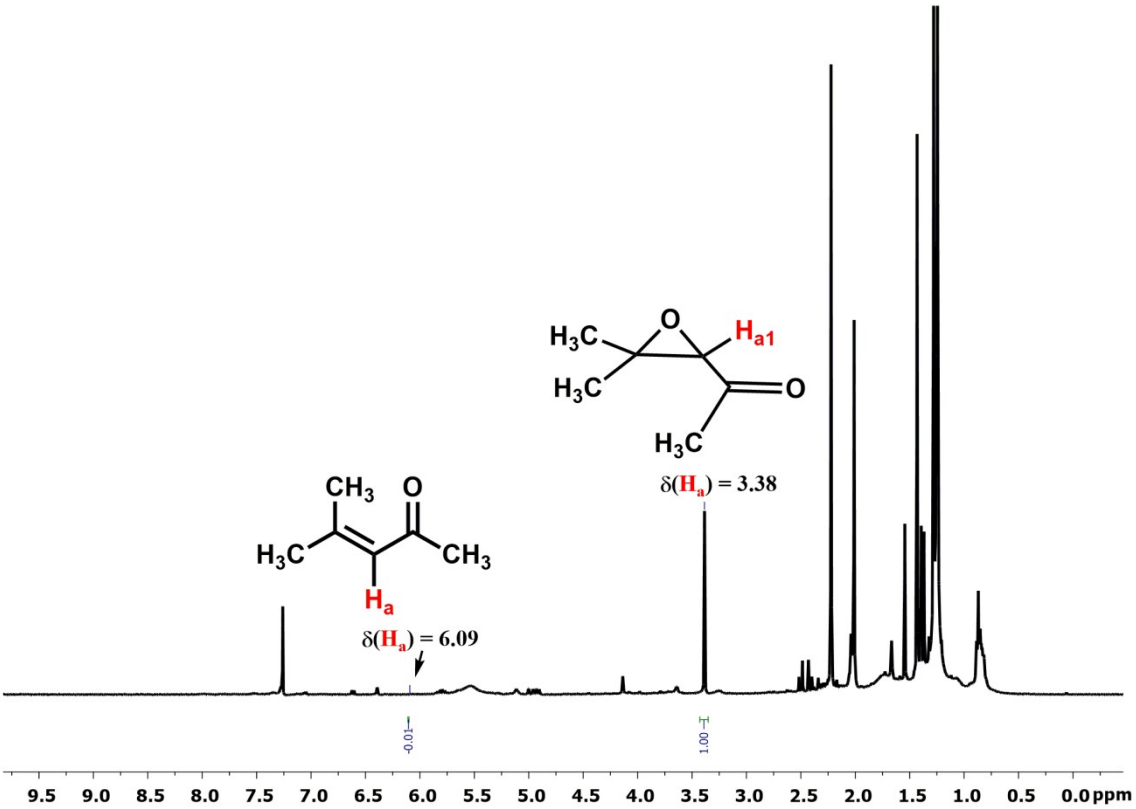

Fig. S20 ^{1}H-NMR spectrum of conversion of 4-methyl-3-penten-2-one to 4-methyl-3-penten-2-one oxide in $CDCl_3$ solution. The reaction was performed in air.

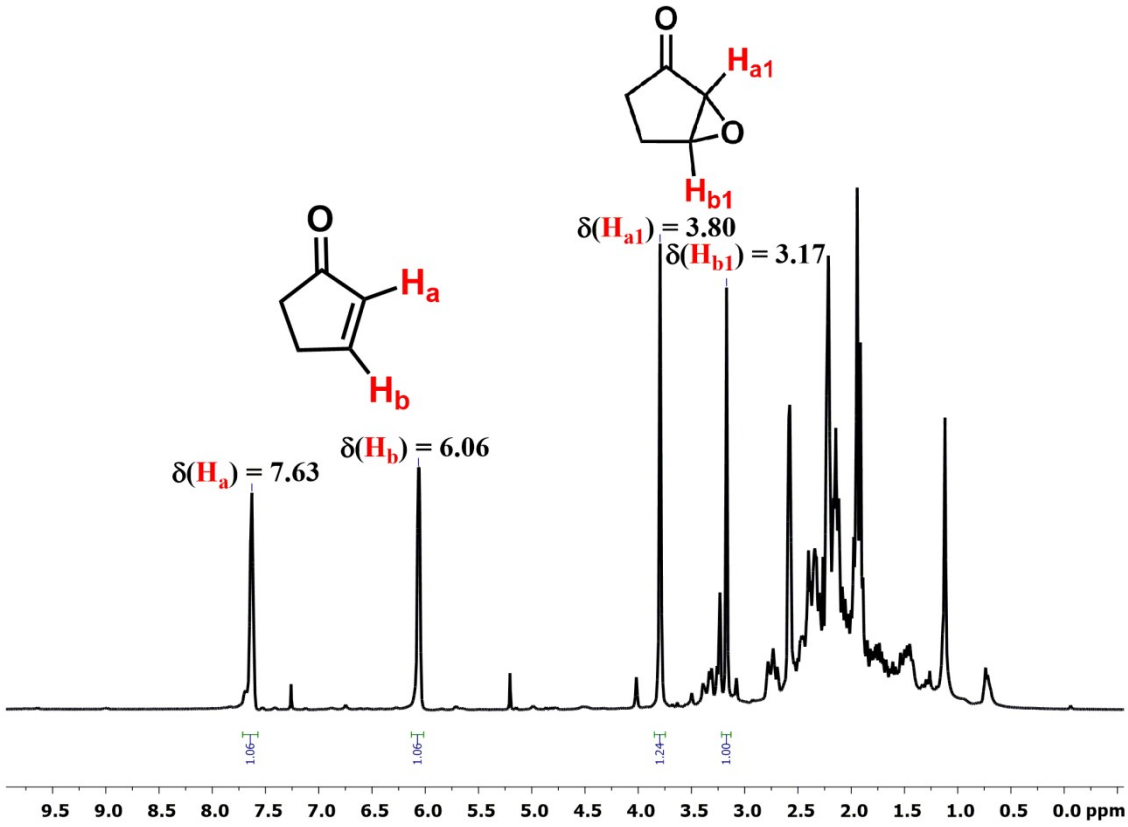

Fig. S21 ^{1}H-NMR spectrum of conversion of 2-Cyclopenten-1-one to 2-Cyclopenten-1-one oxide in $CDCl_3$ solution. The reaction was performed in air.

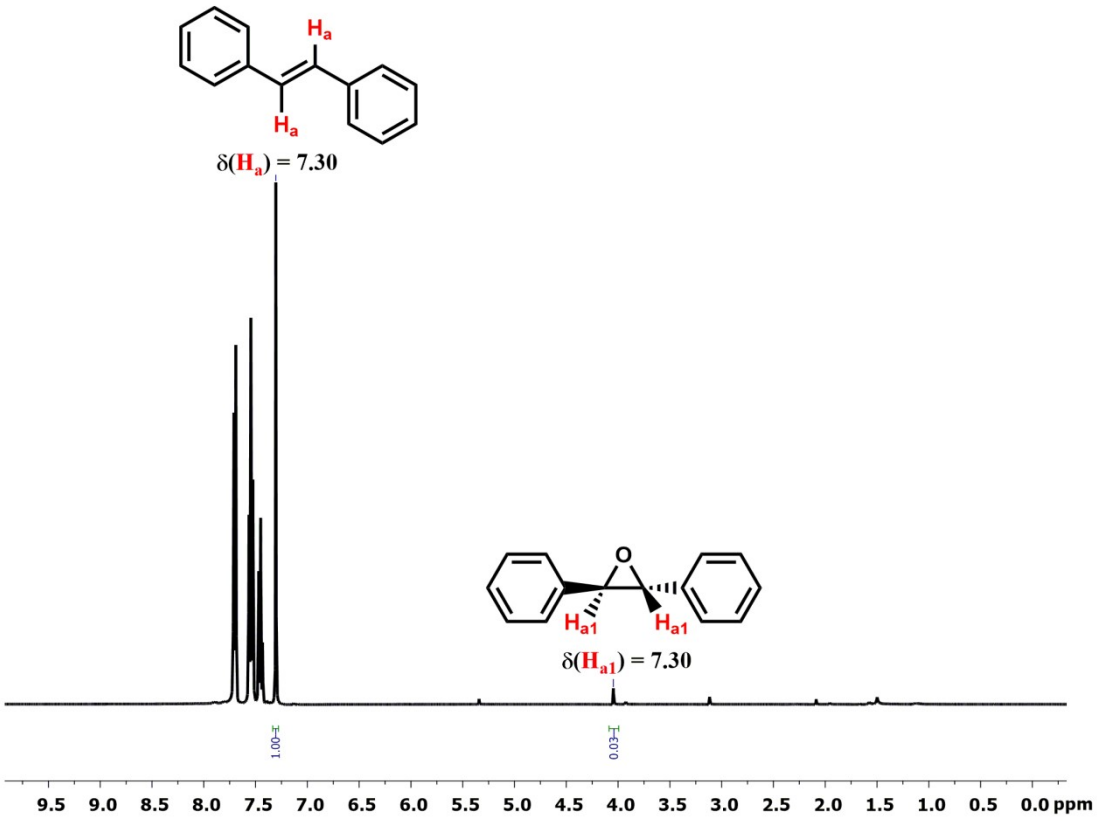

Fig. S22 ^{1}H-NMR spectrum of conversion of *trans*-stilbene to *trans*-stilbene oxide in $CDCl_3$ solution. The reaction was performed in air.

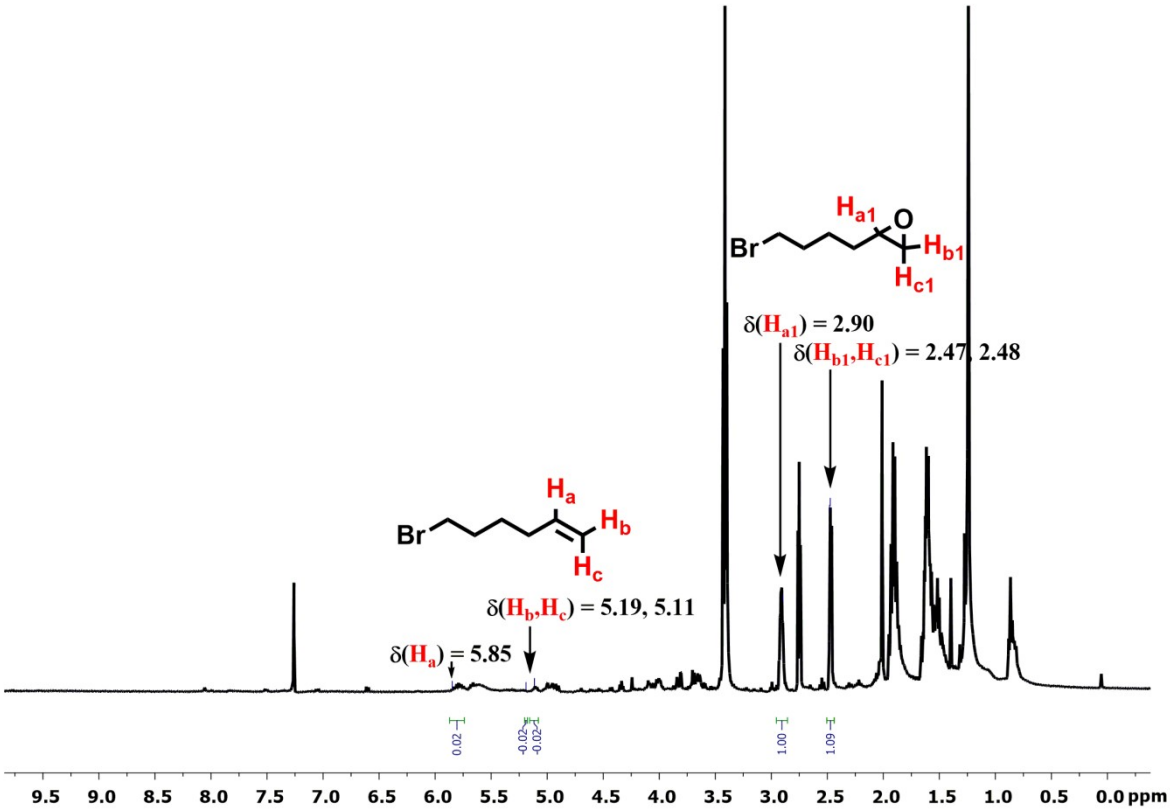

Fig. S23 ^{1}H-NMR spectrum of conversion of 6-bromo-1-hexene to 6-bromo-1-hexene oxide in $CDCl_3$ solution. The reaction was performed in air.

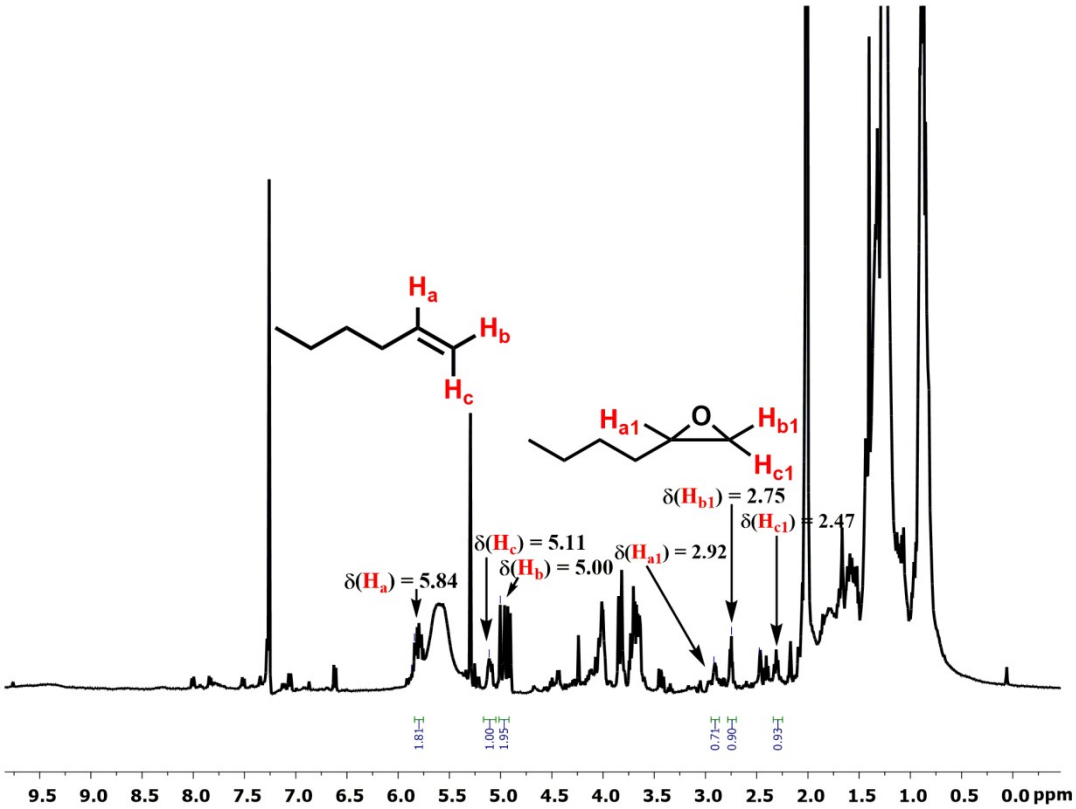

Fig. S24 ^{1}H-NMR spectrum of conversion of 1-hexene to 1-hexene oxide in $CDCl_3$ solution. The reaction was performed in air.

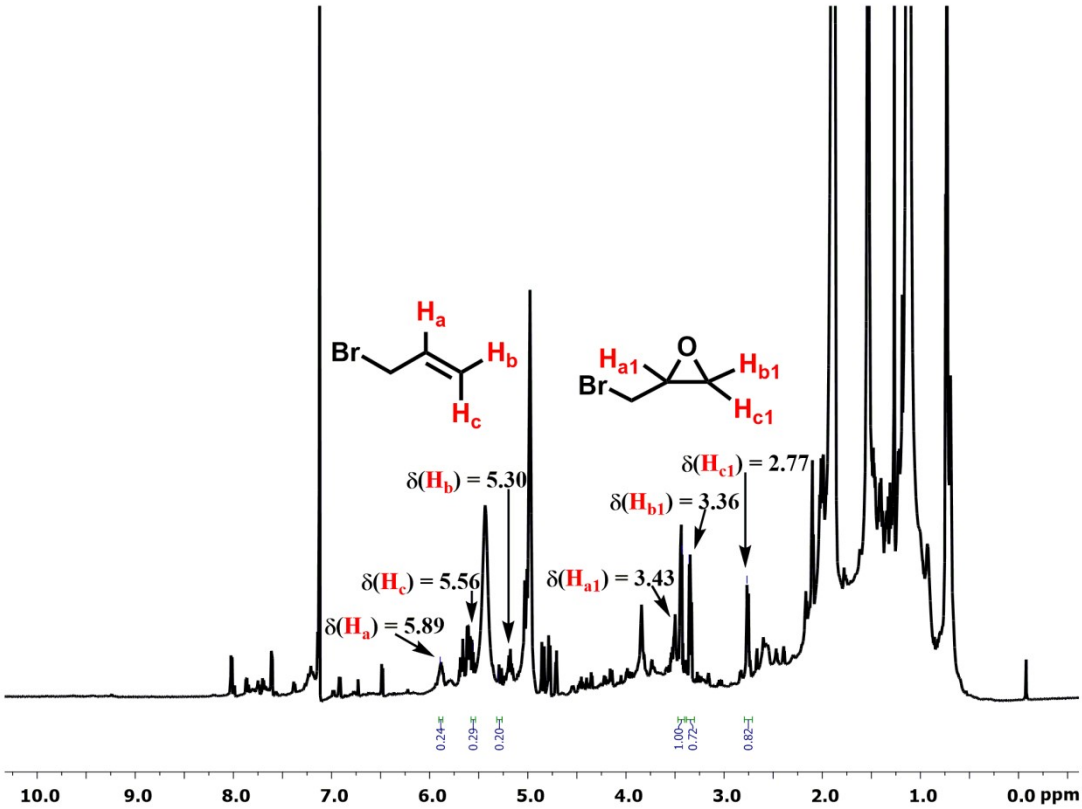

Fig. S25 ^{1}H-NMR spectrum of conversion of 3-bromopropene to 3-bromopropene oxide in $CDCl_3$ solution. The reaction was performed in air.

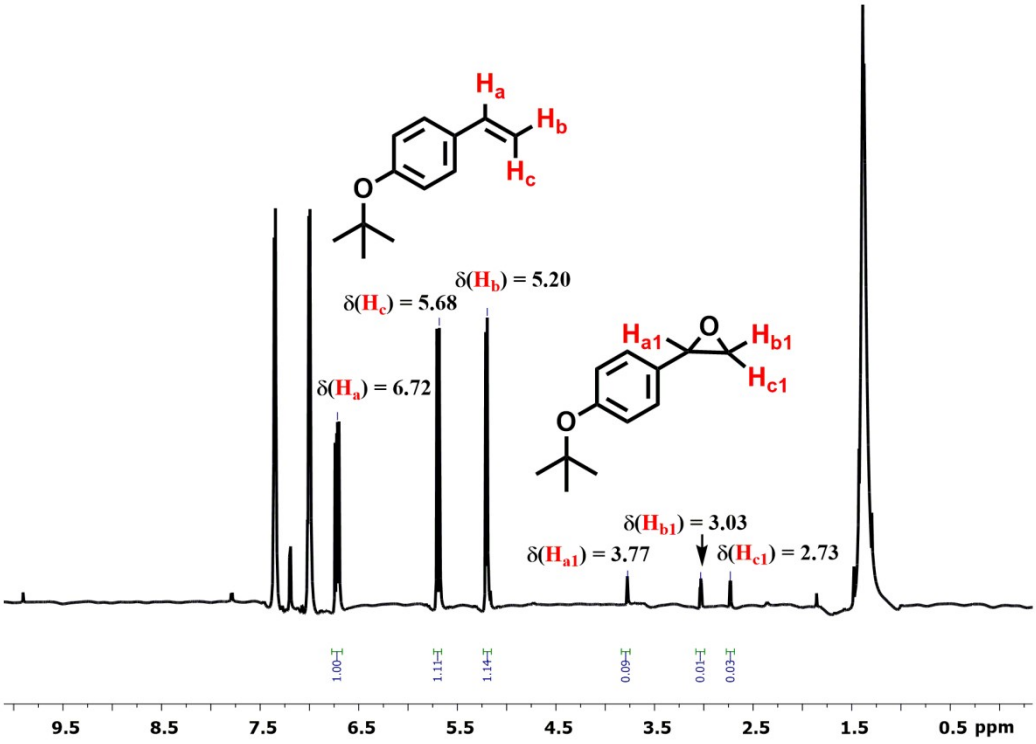

Fig. S26 ^{1}H-NMR spectrum of conversion of 4-*tert*-butoxystyrene to 4-*tert*-butoxystyrene oxide in $CDCl_3$ solution. The reaction was performed in air.

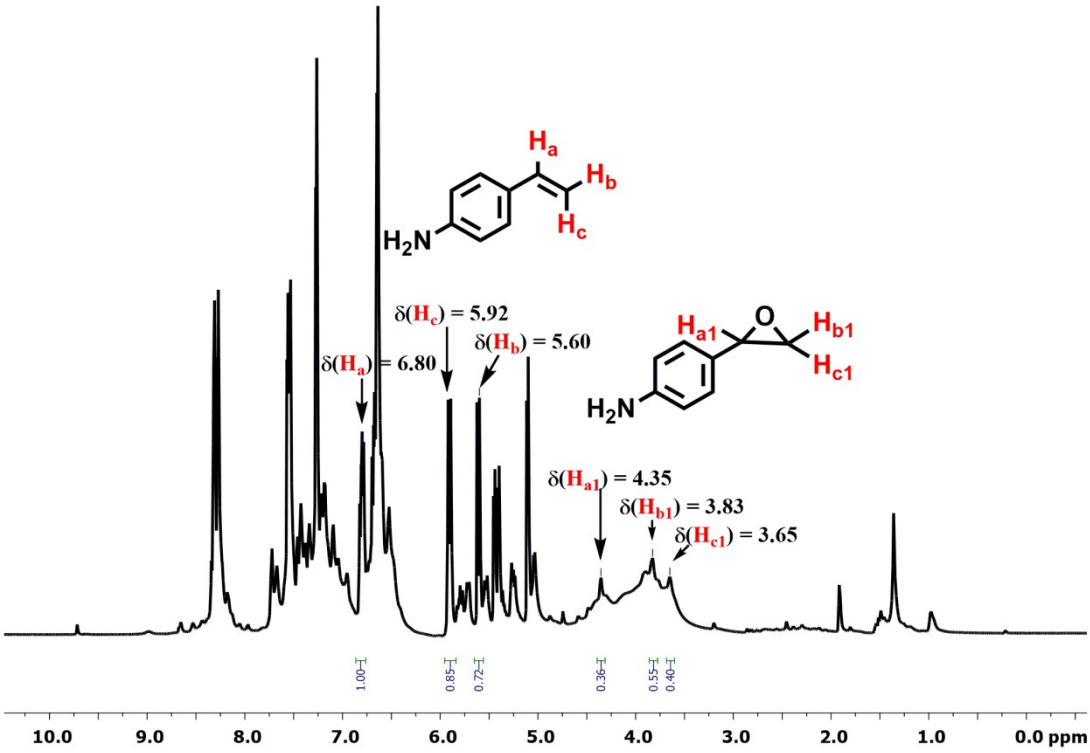

Fig. S27 ^{1}H-NMR spectrum of conversion of 4-vinylaniline to 4-vinylaniline oxide in $CDCl_3$ solution. The reaction was performed in air.

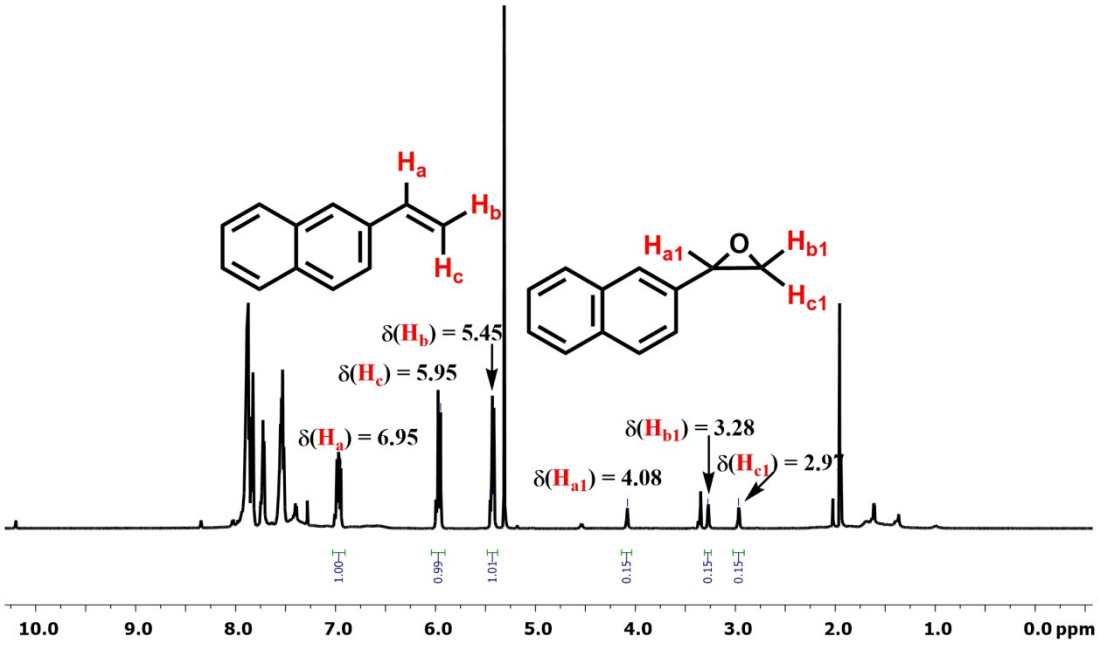

Fig. S28 ^{1}H-NMR spectrum of conversion of 4-vinylnapthalene to 4-vinylnapthalene oxide in $CDCl_3$ solution. The reaction was performed in air.

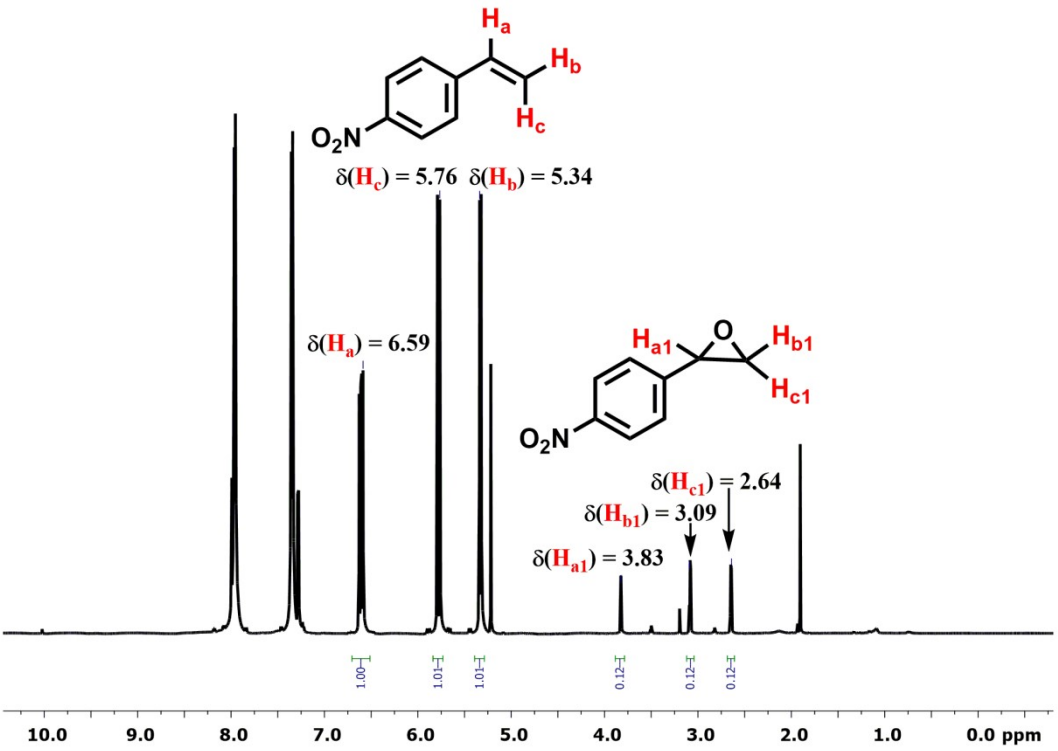

Fig. S29 ^{1}H-NMR spectrum of conversion of 4-nitrostyrene to 4-nitrostyrene oxide in $CDCl_3$ solution. The reaction was performed in air.

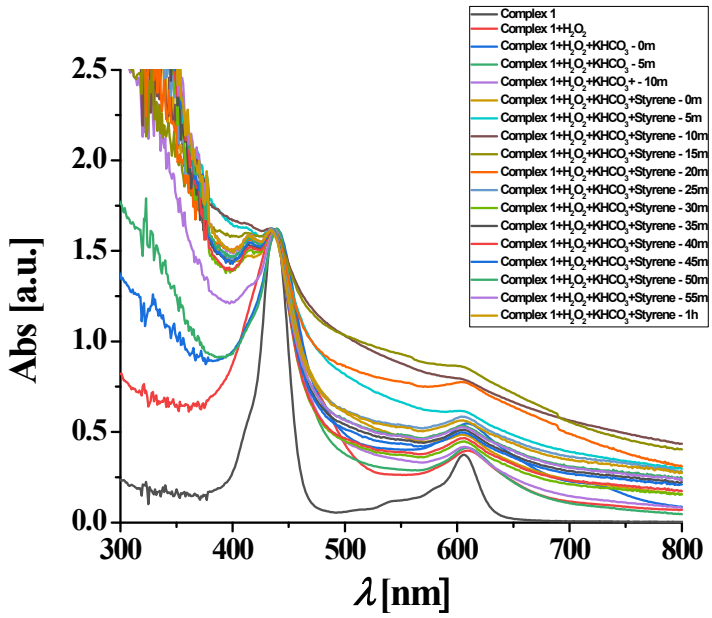

Fig. S30 Time evolution UV−vis spectra of the epoxide formation reaction performed at 50°Cunder air using complex **1** as a catalyst.

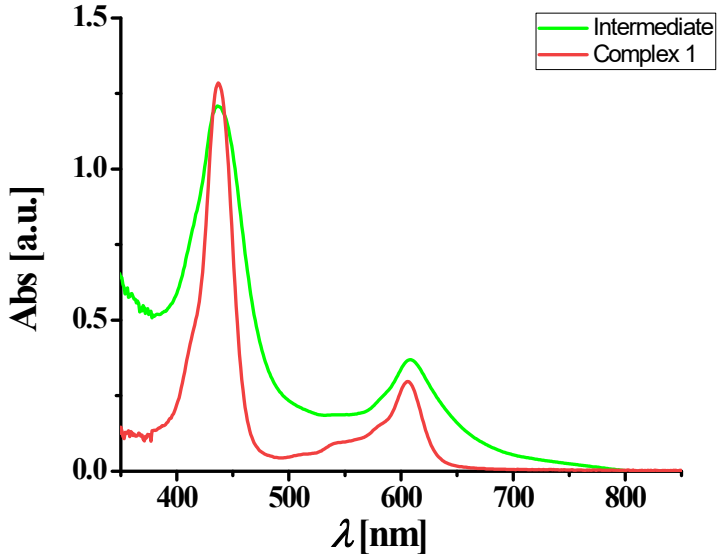

Fig. S31 Electronic absorption spectrum of **1** (red line) and the green intermediate (green line) in acetonitrile. After performing the reaction at 50°C, the pure green intermediate was purified by column chromatography.

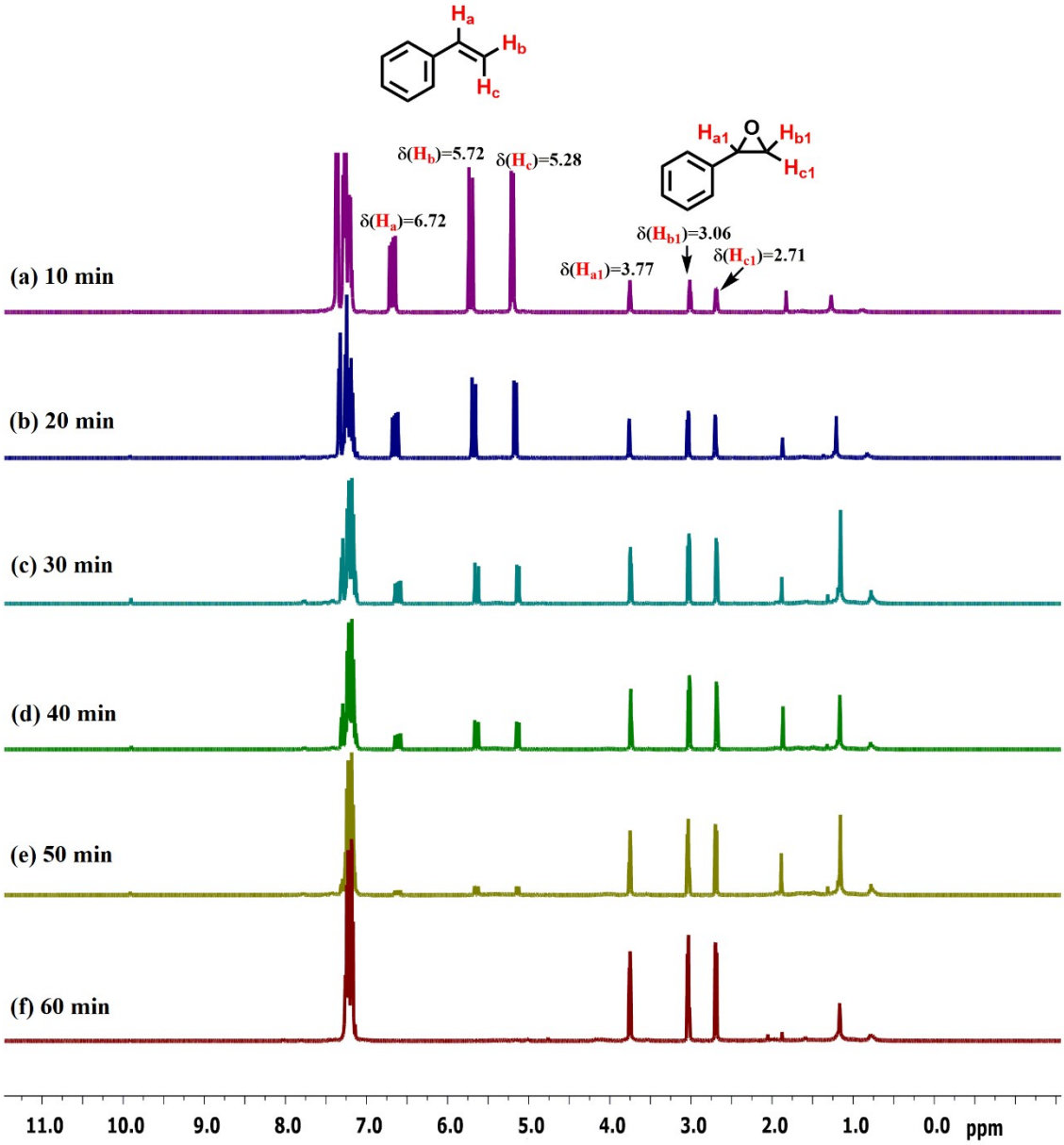

Fig. S32 Time evolution ^{1}H-NMR spectra in CD_3CN of the epoxide formation reaction performed at 50°C under air using complex **1** as catalyst.

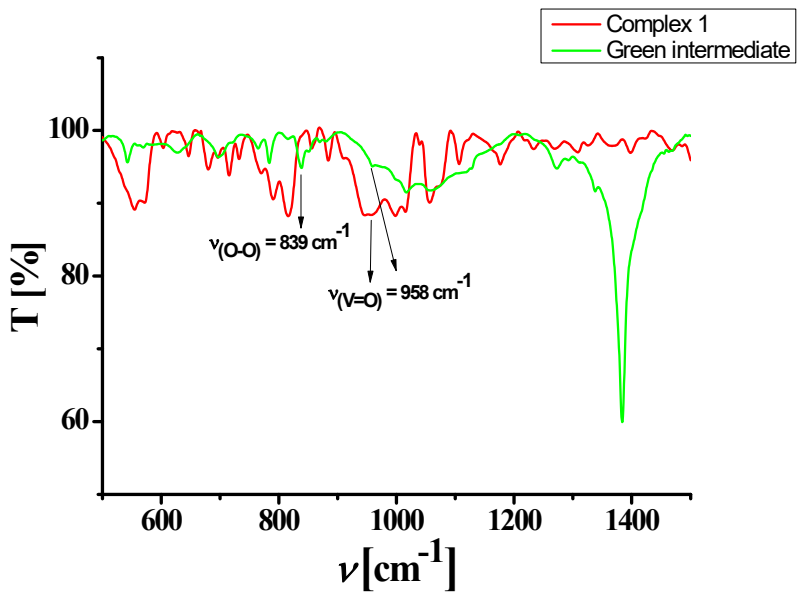

Fig. S33 FT-IR spectrum of **1** (red line) and the green intermediate (green line) as KBr pellet. After performing the reaction at 50°C, the pure green intermediate was purified by column chromatography.

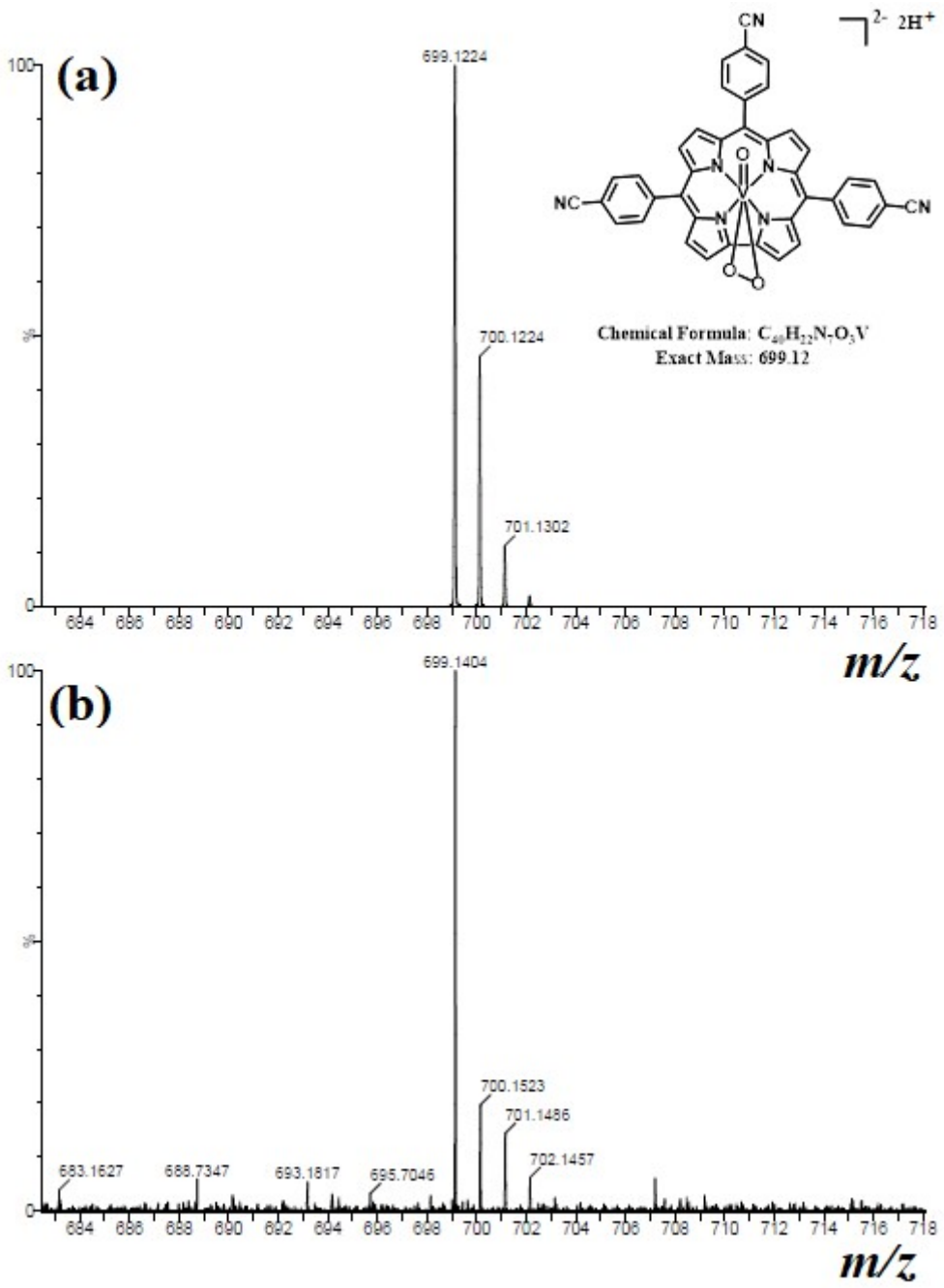

Fig. S34 ESI-MS spectrum of green intermediate, oxo(peroxo)(corrolato)vanadium(V) in CH_3CN shows the (a) isotopic distribution pattern (simulated) and (b) measured spectrum with isotopic distribution pattern (experimental).

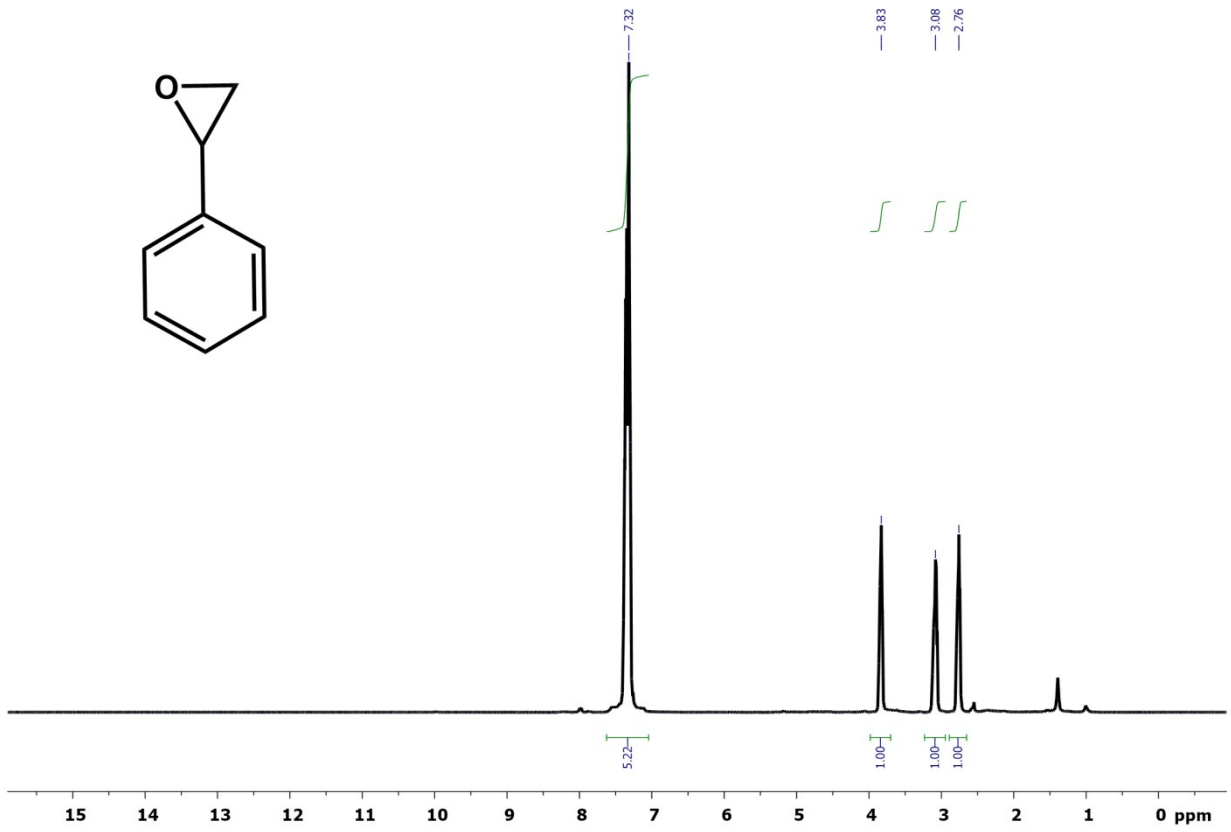

Fig. S35 ^{1}H-NMR spectrum of styrene oxide in $CDCl_3$ solution.

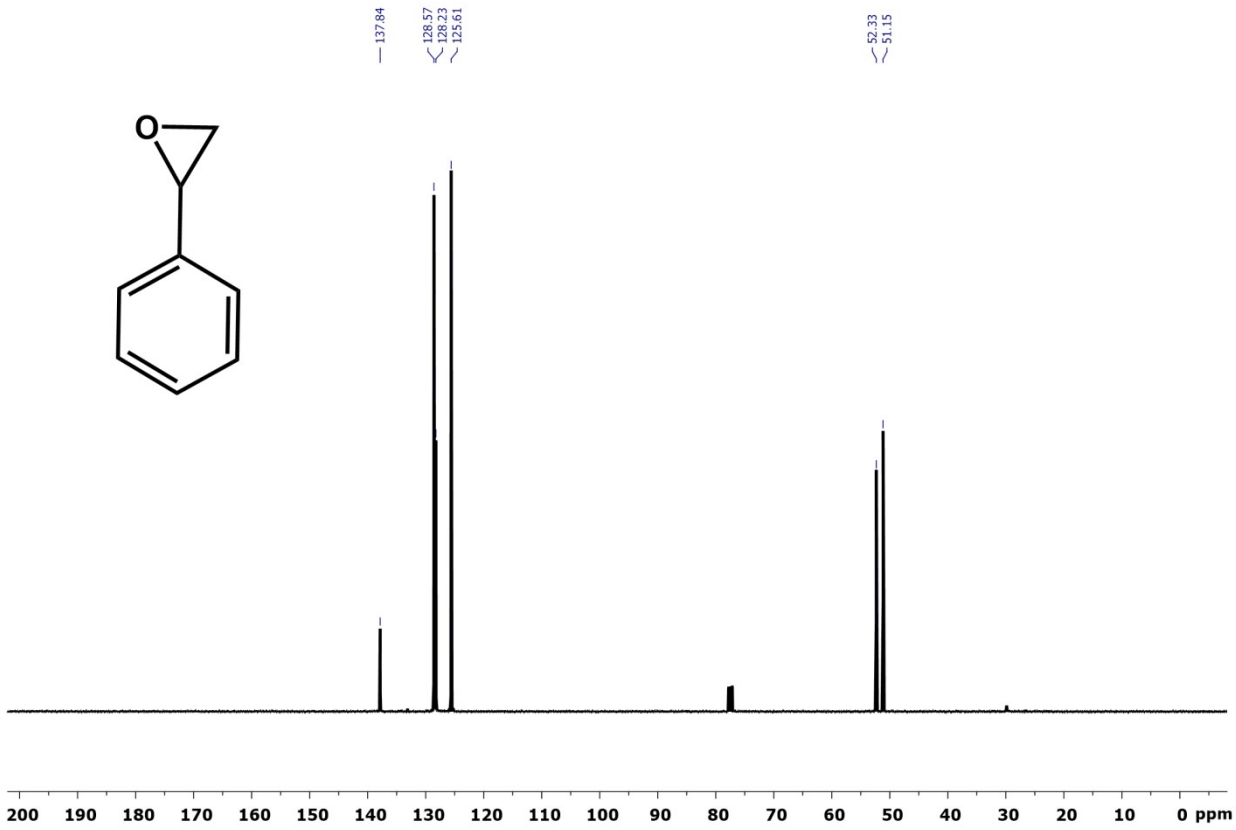

Fig. S36 $^{13}C\ \{^{1}H\}$-NMR spectrum of styrene oxide in $CDCl_3$ solution.

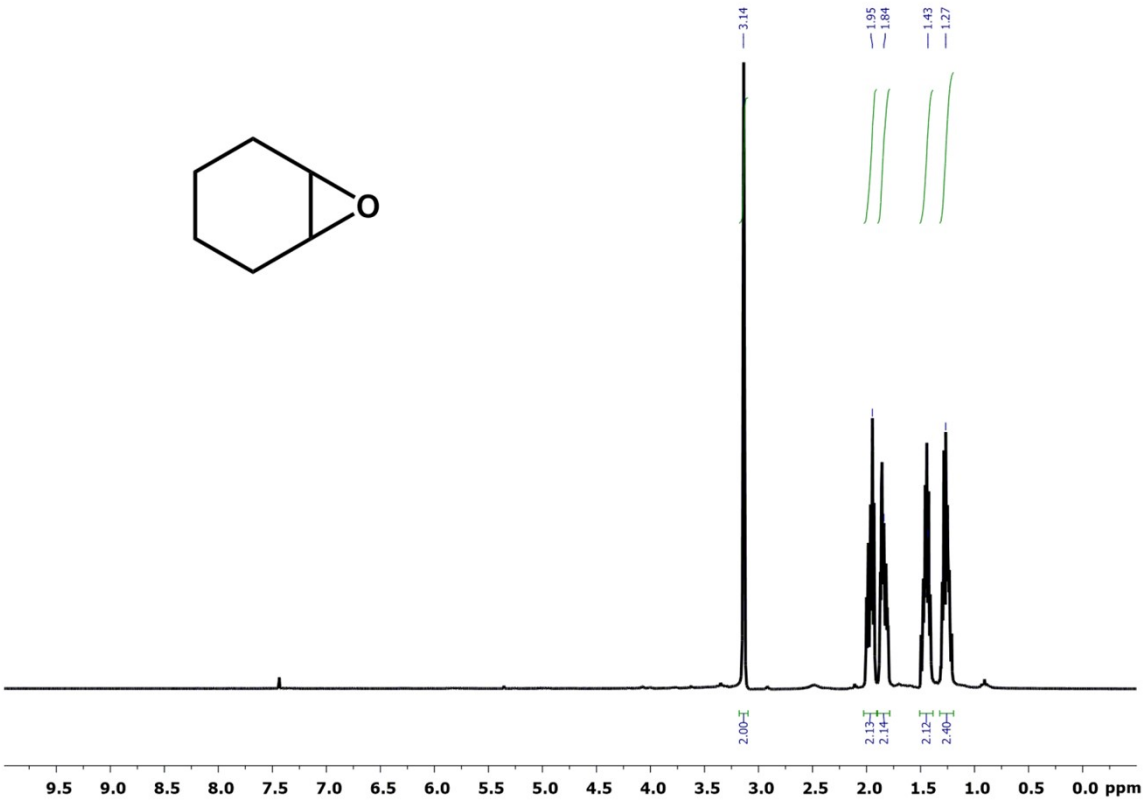

Fig. S37 ^{1}H-NMR spectrum of cyclohexene oxide in $CDCl_3$ solution.

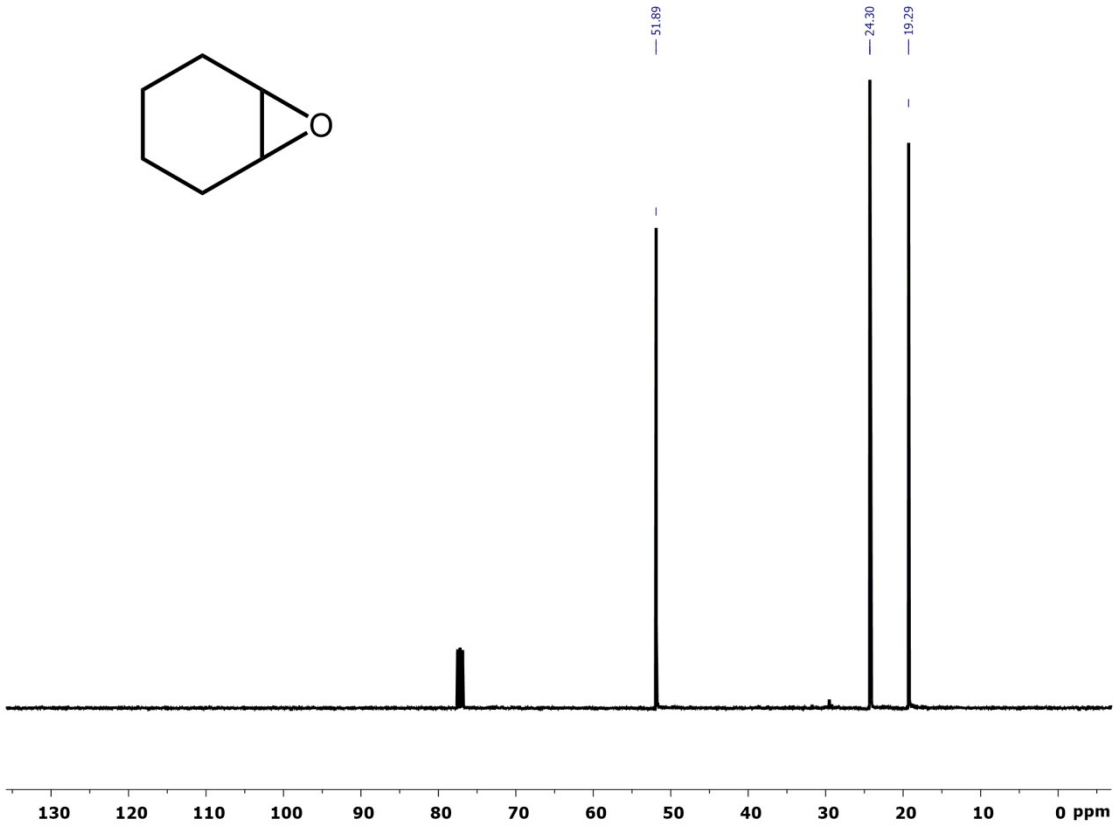

Fig. S38 $^{13}C\ \{^{1}H\}$-NMR spectrum of cyclohexene oxide in $CDCl_3$ solution.

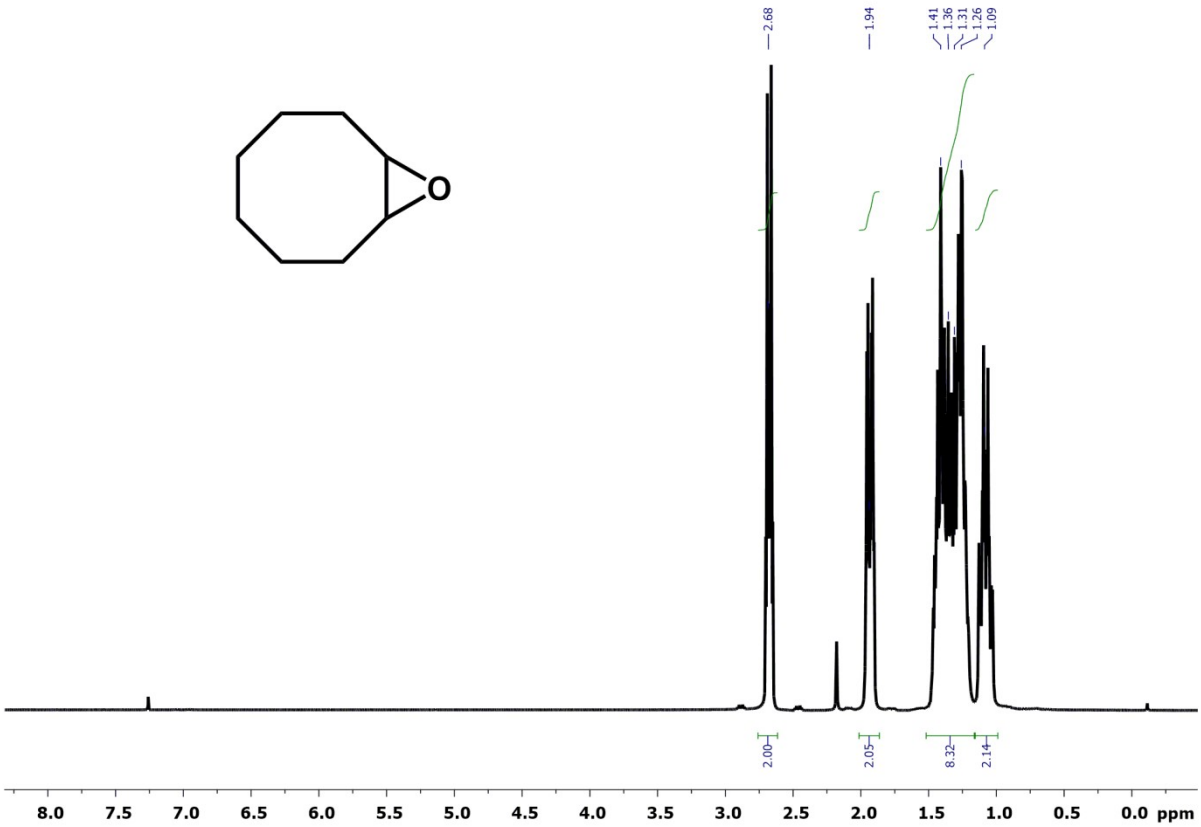

Fig. S39 ^{1}H-NMR spectrum of cyclooctene oxide in $CDCl_3$ solution.

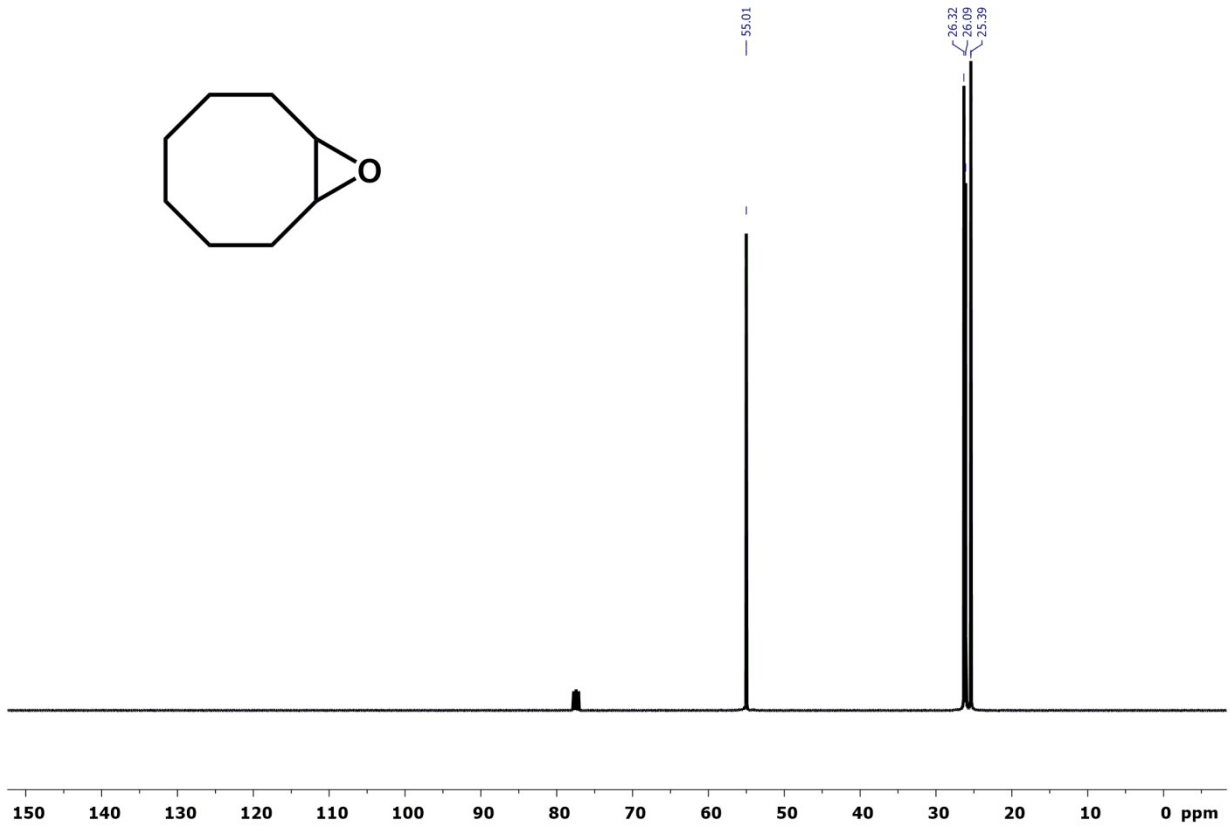

Fig. S40 $^{13}C\ \{^{1}H\}$-NMR spectrum of cyclooctene oxide in $CDCl_3$ solution.